# Mechanism of manganese dysregulation of dopamine neuronal activity

Min Lin[1], Luis M. Colon-Perez[2], Danielle O. Sambo[1], Douglas R. Miller[1], Joseph J. Lebowitz[1], Felix Jimenez-Rondan[3], Robert J. Cousins[3], Nicole Horenstein[4], Tolunay Beker Aydemir[5], Marcelo Febo[2], Habibeh Khoshbouei[1]

[1]Department of Neuroscience, University of Florida, Gainesville, FL 32611
[2]Department of Psychiatry, University of Florida, Gainesville, FL 32611
[3]Center for Nutritional Sciences, University of Florida, Gainesville, FL 32611
[4]Department of Chemistry, University of Florida, Gainesville, FL 32611
[5]Division of Nutritional Sciences, Cornell University, Ithaca, NY 14850

Authors' contributions: M.L. designed and performed experiments, analyzed the data, and wrote the manuscript; L.M.C.P. performed experiments and analyzed the data; D.M. performed experiments; D.S. performed experiments and wrote the manuscript, J.L. performed experiments; F.J.R. performed experiments and analyzed data; R.J.C. designed and performed experiments, analyzed the data, and wrote the manuscript; N.H. performed modeling and wrote the manuscript; T.B.A. designed and performed experiments, analyzed data, and wrote the manuscript; M.F. designed and performed experiments, analyzed data, and wrote the manuscript; H.K. designed experiments, reviewed the data, and wrote the manuscript.

Conflict of interest: The authors do not have a conflict of interest.
Data availability: All data are made publicly available via DRYAD repository.

Corresponding Author:
Habibeh Khoshbouei
Habibeh@ufl.edu

Key words: Manganese, Dopamine Neurons, L-type Calcium Channel, Synaptic Transmission, Parkinson's Disease

## Abstract

Manganese exposure produces Parkinson's-like neurological symptoms, suggesting a selective dysregulation of dopamine transmission. It is unknown, however, how manganese accumulates in dopaminergic brain regions or how it regulates the activity of dopamine neurons. Our *in vivo* studies suggest manganese accumulates in dopamine neurons of the ventral tegmental area and substantia nigra via nifedipine-sensitive $Ca^{2+}$ channels. Manganese produces a $Ca^{2+}$ channel-mediated current which increases neurotransmitter release and rhythmic firing activity of dopamine neurons. These increases are prevented by blockade of $Ca^{2+}$ channels and depend on downstream recruitment of $Ca^{2+}$-activated potassium channels to the plasma membrane. These findings demonstrate the mechanism of manganese-induced dysfunction of dopamine neurons, and reveal a potential therapeutic target to attenuate manganese-induced impairment of dopamine transmission.

## Significance Statement

Manganese is a trace element critical to many physiological processes. Overexposure to manganese is an environmental risk factor for neurological disorders such as a Parkinson's disease-like syndrome known as manganism. We found manganese dose-dependently increased the excitability of dopamine neurons, decreased the amplitude of action potentials, and narrowed action potential width. Blockade of $Ca^{2+}$ channels prevented these effects as well as manganese accumulation in the mouse midbrain *in vivo*. Our data provide a potential mechanism for manganese-regulation of dopaminergic neurons.

## Introduction

Manganese is a trace element critical to many physiological and developmental processes, including the regulation of macronutrient metabolism, blood glucose, cellular energy, reproduction, digestion, and bone growth (Greene and Madgwick, 1988; Erikson et al., 2005). Manganese is a cofactor for several enzymatic processes and a constituent of metalloenzymes, including arginase, pyruvate carboxylase, and manganese-containing superoxide dismutase (Ashner and Aschner, 2005; Ashner et al., 2007; Guilarte, 2010). Except in children on long-term parenteral nutrition or individuals with mutations in the metal transporter SLC39A8 gene, manganese deficiencies are seldom reported (Greene and Madgwick, 1988; Zogzas and Mukhopadhyay, 2017). In contrast, excess manganese accumulation in the brain following environmental exposure is implicated in abnormalities related to the dopaminergic system, including Parkinson-like motor dysfunction (Jankovic, 2005), ataxia (Soriano et al., 2016), and hallucinations (Verhoeven et al., 2011). Animal models of manganism have shown that a single large exposure or prolonged moderate exposure to excess manganese is detrimental to the basal ganglia function (Michalke and Fernsebner 2014; Olanow, 2004), albeit with less understood mechanisms.

Manganese can enter the central nervous system (CNS) through the cerebral spinal fluid or by crossing cerebral capillary endothelial membranes (Aschner et al., 2007). Physiological concentrations of manganese in the human brain range from 20 to 53 μM (Bowman and Aschner, 2014) but can increase several-fold upon overexposure both in humans (Crossgrove and Zheng, 2004; Kessler et al., 2003) as well as rodents (Liu et al., 2006). Existing studies have used a wide range (60–150 μM) of extracellular manganese to investigate manganese-associated neurotoxicity (Bowman and Aschner, 2014; Tuschl et al., 2013). Studies on manganese transport in mammalian systems have largely focused on influx mechanisms (Au et al., 2008). Manganese is transported

into neurons, and possibly other CNS cell types, through a number of transporters, including divalent metal transporters (Gunshin et al., 1997), the transferrin receptor (Gunter et al., 2013), store-operated $Ca^{2+}$ channels (Crossgrove and Yokel, 2005), the choline transporter (Lockman et al., 2001), the magnesium transporter (Goytain et al., 2008), and the NMDA receptor (Itoh et al., 2008). In addition, ZIP14 is shown to uptake manganese in human neuroblastoma cells (Fujishiro et al., 2014). The clinical effects of manganese toxicity are primarily Parkinson-like in nature (Jankovic 2005). This includes movement disorders characterized by tremor, rigidity, dystonia and/or ataxia; psychiatric disturbances including irritability, impulsiveness, agitation, obsessive-compulsive behavior, and hallucinations; and cognitive deficits such as memory impairment, reduced learning capacity, decreased mental flexibility, and cognitive slowing (Josephs et al., 2005). Neuronal degeneration and altered neurotransmitter release occur in brain regions with abnormally high accumulation of manganese, including the dorsal striatum, internal globus pallidus (GPi), and substantia nigra pars reticulata (SNpr) (Crossgrove and Zheng, 2004; Guilarte, 2010; Perl and Olanow, 2007; Uchino et al., 2007). In addition, neuronal loss and gliosis in the globus pallidus, SNpr, and striatum are reported with high accumulation of manganese (Olanow, 2004). Consistently, there is severe cell loss in the substantia nigra pars compacta (SNpc) of individuals with documented chronic manganese exposure, typically through occupational or environmental means (Perl and Olanow, 2007). More recently, mutations in the human metal transporter genes ZNT10 and ZIP14 have shown to cause manganese overload and motor dysfunction (Leyva-Illades et al., 2014; Tuschl et al., 2013). In addition to these clinical findings, previous studies show a correlation between elevated extracellular manganese levels in the brain and dysfunction of dopamine transmission (Dodd et al., 2013; Madison et al., 2012), where manganese reduced dopamine uptake and amphetamine-induced dopamine efflux (Roth et al.,

2013). Manganese exposure in developing rats reduces both the levels and activity of striatal $D_2$ receptors (Seth and Chandra, 1984; Rogers et al., 2014), supporting the overarching hypothesis for manganese-mediated dysregulation of the dopaminergic system.

The mechanism by which manganese dysregulates dopamine neurons is poorly understood. One potential mechanism by which manganese can regulate cellular responses is through the modulation of $Ca^{2+}$ concentrations, which not only regulates membrane potential but also serves as an important signaling molecule (Clapham, 2007). Manganese has been shown to regulate $Ca^{2+}$ signaling in primary astrocytes cultures where exposure to manganese results in mitochondrial sequestration of $Ca^{2+}$ which in turn reduces the available pool of releasable $Ca^{2+}$ within the endoplasmic reticulum (Tjalkens et al., 2006). This can affect the production of reactive oxygen species, free radicals, and toxic metabolites; alteration of mitochondrial function and ATP production; and depletion of cellular antioxidant defense mechanisms (Martinez-Finley et al., 2013; Puskin and Gunter, 1973). In primary astrocytes, manganese rapidly inhibits ATP-induced $Ca^{2+}$ waves and $Ca^{2+}$ transients (Streifel et al., 2013) as well as decreases the influx of extracellular $Ca^{2+}$ induced by 1-oleoyl-2-acetyl-sn-glycerol (OAG), a direct activator of the transient receptor potential channel TRPC3 (Streifel et al., 2013).

The mechanistic relationship between manganese-regulation of $Ca^{2+}$ signaling and excitability of dopamine neurons has remained unclear. Recently, we have shown changes in $Ca^{2+}$ homeostasis in the dopamine neurons influence neuronal activity indirectly through $Ca^{2+}$-activated potassium channels (Lin et al., 2016). In the current study, we report a mechanistic link between manganese regulation of the excitability of dopamine neurons and manganese modulation of $Ca^{2+}$ channels.

Here, we identified a cellular mechanism by which manganese accumulates in the midbrain, influxes into dopamine neurons, and regulates the activity of dopamine neurons. Contrary to our initial hypothesis, we found manganese does not block $Ca^{2+}$ channels in dopamine neurons but acts as a substrate for $Ca^{2+}$ channels. The influx of manganese through the nifedipine-sensitive $Ca^{2+}$ channels was further supported by computational modeling, single neuron analysis, and *in vivo* magnetic resonance imaging experiments showing blockade of Cav1.2 channels decreased manganese regulation of dopaminergic neuronal activity and its accumulation in the midbrain. These data address the existing debate in the field regarding manganese regulation of $Ca^{2+}$ channels in dopamine neurons. The mechanistic results reported here provide a clinically relevant therapeutic target that could attenuate the severity of manganese toxicity in patients exposed to excess manganese.

## Materials and Methods

***Drugs and reagents:*** The drugs and reagents used in this study were purchased from Millipore Sigma-Aldrich (St. Louis, Mo), unless otherwise stated. Chemical reagents and drugs used for primary neuronal culture are listed in Table 1. Antibodies used for Western blot analysis are listed in Table 2. The catalog number of the reagents and drugs used for electrophysiology and microscopy experiments are listed in Table 3.

***Animals*:** Midbrain neuronal cultures were obtained from RFP::TH C57BL/6 mice (obtained from Dr. Douglas McMahon, Vanderbilt University), a transgenic mouse strain where the dopamine neurons are rendered fluorescent by expressing the red fluorescent protein (RFP) under the tyrosine

hydroxylase (TH) promoter (Zhang et al., 2004). Mice conditionally expressing GCaMP6f in dopaminergic neurons were generated by crossing animals expressing Cre recombinase under control of the Slc6a3 promoter (B6.SJL-Slc6a3tm1.1 (cre)BkmnI J; Jackson Lab, Stock: 006660) to animals expressing GcaMP6f under control of the LoxP promoter (B6;129s-Gt(ROSA) 26Sortm95.1 (CAG-GCaMP6f HzeI J; Jackson Lab, stock: 024105). Mice were housed in the animal care facilities at the University of Florida in accordance with Institutional Animal Care and Use Committee, under guidelines established by National Institutes of Health. Food and water were available *ad libitum* in the home cage. Animals were housed under standard conditions at 22−24°C, 50–60% humidity, and a 12 h light/dark cycle.

***Manganese concentrations used in this study:*** The physiological concentration of manganese in the human brain is estimated to be between 5.32 and 14.03 ng manganese /mg protein, equivalent to 20.0–52.8 μM (Bowman and Aschner, 2014). Average cellular manganese content in animal models of chronic manganese exposure is as high as 10.95 μg $g^{-1}$ (200 μM), which was shown to decrease the viability of dopamine neurons (Higashi et al., 2004). Using this information, we first performed dose response experiments (Figure 1 and 2) and found that 100 μM manganese is a suitable concentration to study manganese-regulation of intrinsic firing behavior of dopamine neurons.

Mice were injected intraperitoneally (i.p.) with manganese (II) chloride tetrahydrate (70 mg/kg, $MnCl_2 \cdot 4H_2O$) in a sub-acute treatment based on a published protocol shown to significantly increase manganese concentrations in the basal ganglia (Dodd et al., 2005).

171 ***Neuronal and cells culture*:** Neuronal primary culture was performed as previously described
172 (Saha et al., 2014; Lin et al., 2016; Sambo et al., 2017). Briefly, mouse midbrain dopamine neurons
173 from 0-2 day old pups of either sex were isolated and incubated in a dissociation medium (in mM):
174 116 NaCl; 5.4 KCl; 26 $NaHCO_3$; 25 glucose; 2 $NaH_2PO_4$; 1 $MgSO_4$; 1.3 cysteine; 0.5 EDTA; 0.5
175 kynurenate containing 20 units/mL papain at 34-36°C under continuous oxygenation for 2 hours.
176 Tissue was then triturated with a fire-polished Pasteur pipette in glial medium (in %): 50 minimum
177 essential media; 38.5 heat-inactivated fetal bovine serum; 7.7 penicillin/streptomycin; 2.9 D-
178 glucose (45%) and 0.9 glutamine (200 mM). Dissociated cells were pelleted by centrifugation at
179 500 x g for 10 min and re-suspended in glial medium. Cells were plated on 12 mm round coverslips
180 coated with 100 μg/ml poly-L-lysine and 5 μg/ml laminin in 35 x 10 mm tissue culture Petri
181 dishes. One hour after plating, the medium was changed to neuronal medium: Neurobasal (Life
182 Technologies, Grand Island, NY), 0.9% L-glutamine, 2% B27 and 1 ng/ml GDNF. Neuronal
183 medium was conditioned overnight on cultured glia. The conditioned neuronal medium was
184 supplemented with 1 ng/mL glial cell line-derived neurotrophic factor and 500 μM kynurenate and
185 sterile-filtered before it was added to the neuronal cultures.
186
187 Plasmids for $Ca_v1.2$-GFP and $Ca_v1.3$-GFP were generous gifts from Dr. Gregory Hockerman
188 (Purdue University). Briefly, cDNAs that encode the cytoplasmic II-III inter-domain loop of
189 $Ca_v1.2$ (amino acids 758-903) or $Ca_v1.3$ (amino acids 752-885) were fused to enhanced GFP were
190 constructed in the pEGFP-N1 vector (Clontech, Mountain View, CA). Plasmids were transformed
191 into MAX Efficiency DH5α Competent Cells (Invitrogen, Waltham, MA) and amplified on Luria-
192 Bertani (LB) agar plates with an ampicillin concentration of 50 mg/L. Individual colonies were
193 selected and further amplified in 250 mL LB medium with 50 mg/L ampicillin. Plasmid DNAs

were purified using the Qiagen Plasmid Plus Maxi Kit (Qiagen, Germantown, MD). The integrity of the clones was confirmed by cDNA sequencing and restriction digest analysis.

HEK 293 cells stably expressing $Ca_v1.2$ or 1.3 were generous gift from Dr. Richard B. Silverman (University of Chicago). Cells were maintained in DMEM (ThermoFisher) supplemented with 10% fetal bovine serum (Gemini Cat. No. 100-106), 1.1 mM sodium pyruvate (Sigma-Aldrich Cat. No. S8636-100ML), 0.1 mg/mL Zeocin (InvivoGen Cat. No. ant-zn-1), and 0.05 mg/mL Hygromycin B (A.G. Scientific Cat. No. H-1012-PBS). Additionally, either 0.3 mg/mL G418 (Caisson Labs Cat. No. ABL06-20ML) or 0.2 mg/mL Blasticidin S hydrochloride (Research Products International Cat. No. B12200-0.05) was added for $Ca_v1.2$ or $Ca_v1.3$, respectively. Cells were passaged at 70-85% confluency 24-48 hours prior to experimentation using TrypLE Express Enzyme (Gibco Cat. No. 12604-021).

***$^{54}$Mn uptake:*** Effectene reagent (Qiagen, Valencia, CA) was used for transient transfection of HEK cells with a plasmid vector either empty or containing $Ca_v1.2$ or $Ca_v1.3$ cDNA. Overexpression of $Ca_v1.2$ and $Ca_v1.3$ was assessed by the western blotting 48 hours after transfection (Millipore Sigma). For $^{54}$Mn uptake experiments, following a 48-hour transfection, the cells were washed with Hanks' balanced salt solution (HBSS) and incubated at 37°C in serum-free DMEM containing 40 µM $MgCl_2$ and $^{54}$Mn at 0.18 µCi /mL (PerkinElmer). In some experiments, cells were pretreated with 10 µM Nifedipine 30 minutes before $^{54}$Mn treatment. After incubation with $^{54}$Mn for the times indicated, cells were washed with chelating buffer (10 mM EDTA, 10 mM HEPES, and 0.9% NaCl) and solubilized in 0.2% SDS 0.2 M NaOH for 1 hour. Radioactivity was measured by gamma-ray solid scintillation spectrometry. Protein content was

217 measured colorimetrically with BCA reagent (Pierce-Thermo Fisher Scientific). Results were
218 expressed as counts per minute (cpm) per mg total protein.
219
220 ***Electrophysiological recordings:*** Spontaneous firing activity of midbrain dopamine neurons was
221 examined via whole cell current clamp recordings as previously described (Saha et al., 2014; Lin
222 et al., 2016; Sambo et al., 2017). The neurons were continuously perfused with artificial cerebral
223 spinal fluid (aCSF) containing (in mM): 126 NaCl, 2.5 KCl, 2 $CaCl_2$, 26 $NaHCO_3$, 1.25 $NaH_2PO_4$,
224 2 $MgSO_4$, and 10 dextrose, equilibrated with 95% $O_2$-5% $CO_2$; pH was adjusted to 7.4. Patch
225 electrodes were fabricated from borosilicate glass (1.5 mm outer diameter; World Precision
226 Instruments, Sarasota, FL) with the P-2000 puller (Sutter Instruments, Novato, CA). The tip
227 resistance was in the range of 3-5 MΩ. The electrodes were filled with a pipette solution containing
228 (in mM): 120 potassium-gluconate, 20 KCl, 2 $MgCl_2$, 10 HEPES, 0.1 EGTA, 2 ATP, and 0.25
229 GTP, with pH adjusted to 7.25 with KOH. All experiments were performed at 37°C. To standardize
230 action potential (AP) recordings, neurons were held at their resting membrane potential (see below)
231 by DC application through the recording electrode. Action potential was recorded if the following
232 criteria were met: a resting membrane potential of less than −35 mV and an action potential peak
233 amplitude of >60 mV. Action potential half-width was measured as the spike width at the half-
234 maximal voltage using Clampfit 10 software (Axon instruments, Foster City, CA). Steady-state
235 basal activity was recorded for 2–3 min before bath application of the drug. For experiments
236 involving drug application, each coverslip was used for only one recording. The spontaneous spike
237 activity of midbrain dopamine neurons was obtained by averaging 1 min interval activities at
238 baseline (before manganese) and after 7-10 min of manganese. The relationship between Mn
239 concentration and neuronal firing frequency was fitted according to a Hill equation: $E$ =

$E_{max}Mn^{nH}/(EC_{50} + Mn^{nH})$ where E is the predicted effect of Mn, $E_{max}$ is the maximum effect, *n*H is the slope factor, and the *n*th root of $EC_{50}$ gives an estimate of the midpoint of the activation curve.

***Recording from HEK Cells expressing GFP-α subunits:*** HEK293 cells stably expressing GFP-α subunits where generous gift from Dr. Robert Brenner (University of Texas Health Science Center at San Antonio). The cells were cultured as described previously (Goodwin et al., 2009; Saha et al., 2014; Wang et al., 2009). The cells were plated on glass coverslips (Electron Microscopy Sciences, Hatfield, PA). Green fluorescent protein expression was used to identify α subunits-expressing cells. Electrophysiology experiments were performed 3 days after plating the cells. Macropatch recordings were performed using the excised inside-out patch clamp configuration at 22 - 23°C. Patch pipettes were pulled to a final tip resistance of 1.5–3 MΩ and filled with the internal solution. The electrode solution was composed of the following (in mM): 20 HEPES, 140 $KMeSO_3$, 2 KCl, and 2 $MgCl_2$, pH 7.2. Bath solution was composed of a pH 7.2 solution of the following (in mM): 20 HEPES, 140 $KMeSO_3$, and 2 KCl. Intracellular $Ca^{2+}$ was buffered with 5 mM HEDTA to give the required 10 μM free [$Ca^{2+}$] concentration calculated using the MAXCHELATOR program (Winmaxchelator software; Dr. Chris Patton, Stanford University, Pacific Grove, CA). Recordings and data acquisition were described in *Single-channel recordings above*. Mean current density was plotted against membrane potential (*I–V*) and was fitted by the Boltzmann equation: $I = I_{min} + (I_{max} - I_{min})/(1 + \exp - \kappa(V - V_{1/2}))$, where *I* is the current, $I_{max}$ is the maximum current, $I_{min}$ is the minimum current, κ is a slope factor, and $V_{1/2}$ is the midpoint potential.

263 ***Pharmacological isolation of $Ca^{2+}$ currents:*** For whole-cell recordings, we used a Cesium
264 methanesulfonate-based intracellular solution composited in mM: 110 $CsMeSO_3$, 10 TEA-Cl, 10
265 4-aminopyridine (4-AP), 10 HEPES, 1 $MgCl_2$, 10 EGTA, 2 ATP and 0.3 GTP, with pH adjusted
266 to 7.25 with CsOH. Bath solution contained following (in mM): 110 NaCl, 35 tetraethylammonium
267 (TEA)-Cl, 1 CsCl, 1 $MgSO_4$, 2 $CaCl_2$, 10 HEPES, 11.1 dextrose and 0.001 tetrodotoxin (TTX),
268 pH 7.4 with CsOH. For the $Ca^{2+}$-free bath solution, 2 mM $CaCl_2$ was replaced with 3 mM $MgCl_2$,
269 a HEPES solution containing 4 mM $Mg^{2+}$. Calcium currents were evoked by a series of 200-ms
270 depolarizing steps from −60 to +85 mV in 5-mV increments. To avoid possible interference
271 between responses, the depolarizing voltage steps were delivered every 5 s. Data were obtained in
272 1- to 3-min intervals while the patches were held at −65 mV. The series resistances were in the
273 range of 5–10 MΩ (typically 5 MΩ) and were compensated 60% on-line. Membrane potential
274 measurements were not corrected for the liquid junction potential (~15 mV). Leak currents were
275 subtracted using a standard P/4 protocol. Before seals (5 GΩ) were made on cells, offset potentials
276 were nulled. Capacitance subtraction was used in all recordings. To determine current density (pA
277 / pF), the peak current value of the steady-state current at 180 ms was divided by the membrane
278 capacitance from each recorded cell.
279
280 ***Preparation of mouse brain slices:*** Unless otherwise noted, 30-40 day-old C57BL/6 male mice in
281 either wild type or mice conditionally expressing GCaMP6f in dopaminergic neurons (described
282 above) were used for slice preparation. Only males heterozygous were selected and used for these
283 experiments. Mice were deeply anesthetized with 4% isoflurane, and the brain was subsequently
284 removed from the cranium. The tissue was glued onto the cutting stage and submersed in ice-cold,
285 oxygenated aCSF (equilibrated with 95% $O_2$-5% $CO_2$). Coronal or horizontal brain slices (200 μm)

containing the substantia nigra compacta or striatum were cut using a MicroSlicer Zero 1N (Dosaka, Kyoto, Japan).

***FFN200 loading and multiphoton imaging****:* Striatal slices of wild type mice were incubated in oxygenated aCSF with 10 µM FFN200 (Tocris, Minneapolis, MN) for 30 min at 22–24° C and washed for 45–50 min before imaging. After incubation with FFN200, dorsal striatal slices were transferred into imaging chambers, then continuously perfused with aCSF equilibrated with 95% $O_2$-5% $CO_2$. *In vitro* multiphoton imaging was performed with a Nikon AR1 MP (Nikon Instruments Inc., Melville, NY, USA) equipped with a plan apo LWD 25x, water-immersion (NA=1.1, WD=1.43 - 2.04mm, DIC N2) objective. Multiphoton excitation was generated with a Spectra Physics 15 W Mai Tai eHP tunable Ti:sapphire femtosecond pulsed IR laser. FFN200 imaging experiments were performed using excitation wavelengths of 830-840 nm and an emission of 430–470 nm. Emission light was directed with a 405 nm dichroic mirror through a 340 nm short pass filter to enhanced hybrid PMTs via fluorophore specific filters. Imaging sites in time lapse experiments were aligned based on the multiphoton imaged dendritic structure and FFN200 puncta. Imaging sites in time lapse experiments were aligned based on the multiphoton imaged dendritic structure and FFN200 puncta. Images were collected with a 2.4 µs pixel dwell time, with the laser attenuated to 3% of total power, a pixel size of 0.24 µm (XY), and a step size of 0.5 µm (Z) at 1,024 × 1,024 pixel resolution. After acquiring an initial image (t = 0), perfusion was switched to aCSF containing 100 µM $MnCl_2$ and images acquired every 4s. Control slices labeled with FFN200 were imaged 5 – 10 min in the absence of $MnCl_2$.

Two photon images and analysis of fluorescent intensity for FFN200 puncta were performed using NIS-Elements Software v4.5 (Nikon Instruments Inc., Melville, NY, USA). Regions of interest

(ROIs) were automatically selected by the program. Background fluorescence intensity was determined as the mean fluorescence intensity of areas of the image that excluded puncta. The mean background-subtracted fluorescent puncta intensity was then calculated by subtracting the mean background intensity from the mean fluorescence intensity measured at the puncta.

***Fura-2 calcium imaging****:* For Fura-2 calcium imaging, primary cultured midbrain neurons (8-10 DIV) were used in all studies. Neurons were washed twice in HBSS (Life Technologies) followed by 30-min treatment in 5 μM Fura-2 AM (Thermo Fisher). Cells were then washed twice with HBSS followed by 30-min incubation in HBSS. Cells were then imaged on a Nikon Ti Eclipse inverted microscope. Fluorescence was monitored using dual excitation wavelengths (340/380 nm) and a single emission wavelength (510 nM). Fura-2 bound to free calcium is excited at 340 nm, whereas unbound Fura-2 is excited at 380 nm. Baseline images were taken for 30 s to 1 min followed by addition of vehicle, 100 μM manganese, or 20 mM caffeine as the positive control group. The concentration of caffeine used in this study was selected based on a previous study examining caffeine-regulation of $Ca^{2+}$ mobilization in the midbrain dopamine neurons (Choi et al., 2006). Images were acquired for 4 min after treatment. For analysis, experimenter defined regions of interest (ROIs) were drawn along the cell body of each neuron. $Ca^{2+}$ changes were determined as the fluorescence normalized to the average fluorescence of the first 30 s of baseline imaging for each neuron. The percent fluorescence change over baseline was calculated as: $\%_{\Delta}F/F_0 = (F_{max}-F_0)/F_0$ x 100, where $F_{max}$ is the maximal fluorescent value after treatment and $F_0$ is the average fluorescence at baseline. Images were presented as the ratio of 340/380 imaging.

***Total internal reflection fluorescence microscopy (TIRFM):*** For these experiments, HEK293 cells expressing GFP-α subunits were plated onto 35 mm glass-bottom dishes (No. 1 thickness) to 60-80% confluence. Nikon Ti Eclipse (Nikon, Melville, NY) inverted microscope equipped with a multi-line solid-state laser source (470, 514, 561nm) was used for all TIRFM imaging. Lasers were guided through a 60X 1.4 NA objective. Images were detected digitally using a CCD camera. Image exposure time was coupled with stimulation duration at 100 ms and laser intensity was maintained at 40%. For quantification of fluorescence intensity at the cell surface, experimenter-defined ROIs were created for each cell in order to exclude both cell membrane overlap between adjacent cells and measurement of intensity at the peripheral edges of cells. Background fluorescence was subtracted from all images. Mean intensity over time for each ROI was recorded continuously before and after the application of 100 μM manganese to the bath solution. Experiments were performed in the isotonic, isosmotic external solution described above. The baseline fluorescent intensity is defined as the average fluorescent intensity 1 min prior to drug application. All values were normalized to the baseline fluorescent intensity. Single count elementary sequential smoothing was applied for image presentation only, and not for analysis. Bleaching at each experimental time point was determined by the amount of decreased fluorescence intensity in untreated cells.

***Magnetic Resonance Imaging Scans****:* Seventeen adult male mice (35-40 days-old male wild-type C57BL/6 mice) were randomly assigned to two groups either receiving manganese only or manganese plus nifedipine. Systemic injections of L-type $Ca^{2+}$ channel inhibitor, nifedipine (15 mg/kg), which can effectively cross the blood–brain barrier (Cain et al., 2002), were used to inhibit the L-type $Ca^{2+}$ channels (Jinnah et al., 1999). The treatment doses were based on the previously

published protocols (Cain et al., 2002, Dodd et al., 2005, Jinnah et al., 1999). Both groups were intraperitoneal (i.p.) injected with manganese (II) chloride tetrahydrate (70 mg/kg), but one group received manganese injection after 30 min nifedipine (15 mg/kg, i.p) injection. Magnetic resonance (MR) scanning was performed twenty-four hours after manganese exposure. On the scanning day, mice were induced using 3-4% isoflurane delivered in medical grade air (70% nitrogen, 30% oxygen; air flow rate 1.5 mL/min). The anesthesia was maintained at 1.0-1.5% isoflurane during MRI scanning. Core body temperature and spontaneous respiratory rates were continuously recorded during MRI scanning (SA Instruments, Stony Brook, NY). Mice were maintained at normal body temperature levels (37– 38 °C) using a warm water recirculation system. The MEMRI scans were collected in a 4.7T/33 cm horizontal bore magnet (Magnex Scientific) at the Advanced Magnetic Resonance Imaging and Spectroscopy facility in the McKnight Brain Institute of the University of Florida. The MR scanner consisted of a 11.5 cm diameter gradient insert (Resonance Research, Billerica, MA, USA) controlled by a VnmrJ 3.1 software console (Agilent, Palo Alto, CA, USA). A quadrature transmit/receive radiofrequency (RF) coil tuned to 200.6 MHz $^{1}$H resonance was used for B1 field excitation and RF signal detection (airmri; LLC, Holden, MA). The MEMRI included a multiple repetition time sequence to calculate parametric $T_1$ maps for each group using a fast spin echo sequence with a total of four TR's (0.5, 1.08, 2.33, 5.04 seconds), and TE = 6.02 ms with the following geometric parameters: 16 x 16 mm$^2$ in plane, 14 slices at 0.8 mm thickness per slice, data matrix = 128 x 128 (125 μm in-plane resolution).

***MRI Post-Processing:*** Whole brain masks were obtained via automatic segmentation with PCNN using high-resolution anatomical scans to remove non-brain voxels. All cropped data were used to create templates for each cohort using Advanced Normalization Tools (ANTs;

377 http://stnava.github.io/ANTs/). The templates were then registered to an atlas of the mice brain
378 using the FMRIB Software Library linear registration program flirt (Jenkinson et al., 2002). The
379 atlas was then transformed back to each individual data set with the registration matrices from
380 ANTS. To generate parametric T1 maps, multi-TR images were fit to the equation $S_{TR}=S_0(1-e^{-TR/T1})$
381 using non-linear regression in QuickVol II for ImageJ (Schmidt et al., 2004). From T1 maps,
382 the T1 relaxation rate (R1 in $ms^{-1}$) is calculated and exported from regions of interest. These
383 methods allowed the measurement of the amount of activity, along with the location of manganese
384 uptake in both the control and drug exposed groups.
385
386 ***Data acquisition and analysis:*** The reported "n" for each experiment is obtained from at least
387 three independent biological replicates. All statistical analyses were performed on data presented
388 in the manuscript are stated in the figure legends and detailed in the methods and the results section.
389 For each experiment, statistical tests were chosen based on the structure of the experiment and data
390 set. No outliers were removed during statistical analysis. Sample sizes estimates were based on
391 published biological, biochemical and electrophysiological literature that utilized the animal
392 model; this was within a range commonly employed by researchers in our field using similar
393 techniques. The electrophysiology data were acquired using the ClampEx 10 software (Molecular
394 Devices). The data were analyzed off-line using pClamp 10. For all experiments, the data are
395 presented as mean ± SEM. N denotes the number of neurons, cells, or mice for each experiment.
396 Statistical significance was assessed using two-tailed Student's *t* tests or one-way ANOVA. If
397 ANOVA showed statistical significance, all pairwise *post hoc* analysis was performed using a
398 Tukey's *post hoc* test. Differences were considered significant at $P < 0.05$. * denotes significance
399 $p < 0.05$. ** denotes significance $p < 0.01$. The coefficient of variation is a measure of the relative

spread of the data. It is computed as the standard deviation divided by the mean times 100%. SigmaPlot 11 was used for all statistical analysis.

## Results

We exploited multiple complementary approaches to identify dopamine neurons for the electrophysiological recordings, as described previously (Lin et al., 2016). A total of 149 midbrain dopamine neurons were recorded and analyzed as outlined below. The primary parameters of passive membrane and action potential were averaged in 30 randomly selected cells. The average resting membrane potential was −48.3 ± 1.1 mV; input resistance was 252.5 ± 21.9 MΩ; membrane time constant was 826.9 ± 52.5 μs; and membrane capacitance was 64.1 ± 3.3 pF.

**Manganese altered the intrinsic firing behavior of midbrain dopaminergic neurons.** Spontaneous firing activity of dopamine neurons was measured before and after manganese application at concentrations of 10, 30, and 100 μM (Figure 1). Lower concentrations of 10 and 30 μM are within the normal range of intracellular manganese (Bowman and Aschner, 2014), whereas 100 μM falls within the pathological range (Gandhi et al., 2018). Acute exposure to manganese increased the spontaneous firing frequency and suppressed the amplitude of action potentials (AP) (red arrows) in a concentration-dependent manner. Superimposed representative traces of spontaneous spikes before (black trace) and after 100 μM manganese (red trace) exposure revealed that manganese increased the firing frequency of dopamine neurons and truncated AP amplitudes (Figure 2A). The $EC_{50}$ for the manganese-mediated increase in firing frequency of dopamine neurons was determined to be 80.2 μM by fitting a concentration-dependent curve using

a Hill equation (Figure 2B). While manganese induced a modest membrane depolarization at lower concentrations ($P > 0.05$), it significantly depolarized membrane potential at the highest concentration tested in this study (100 μM), which is consistent with the reported manganese concentration for *in vitro* studies (Bowman and Aschner, 2014) (Figure 2C; baseline: -48.1 ± 1.2 mV; 400 μM manganese: -41.8 ± 3.1 mV; $t_{(15)} = -2.2$, $p = 0.045$, two-tailed Student's t tests; $n = 7$ vs 10). Although manganese markedly suppressed AP amplitude at the lowest dose of 10 μM (baseline: 37.2 ± 1.1 mV; 10 μM manganese: 31.1 ± 1.1 mV; $t_{(15)} = 3.6$, $p = 0.03$, two-tailed Student's t tests; $n = 11$ vs 6), higher doses of manganese did not further suppress AP amplitude (Figure 2D). In contrast, manganese did not influence AP half-width at low concentrations, but it significantly narrowed AP width at 100 μM (Figure 2E, baseline: 1.5 ± 0.1 ms; 100 μM manganese: 1.15 ± 0.1 ms; $t_{(15)} = 2.2$, $p = 0.04$, two-tailed Student's t tests; $n = 10$ vs. 7). Manganese progressively decreased the coefficient-of-variation (CV) from 50 μM, indicating a reduction in firing variation evident by the small interspike interval (Figure 2F, baseline: 1.2 ± 0.1; 200 μM manganese: 0.7 ± 0.1 ms; $t_{(22)} = 3.4$, $p = 0.003$, two-tailed Student's t tests; $n = 11$ vs 13). These results suggest manganese can regulate the intrinsic firing behavior of dopamine neurons at both physiological and pathophysiological concentrations in a concentration-dependent manner. To address the pathological effects of manganese, 100 μM was used for the rest of the study based on the determined $EC_{50}$ in Figure 2B.

**Manganese-stimulation of neuronal activity increased the release of fluorescent false neurotransmitter (FFN200).** Next, we asked whether manganese-stimulation of firing frequency of dopamine neurons leads to increased neurotransmitter release. To do this, we utilized FFN200, a fluorescent substrate of VMAT2 that selectively traces monoamine exocytosis in both neuronal

446 culture and striatal slices (Pereira et al., 2016). "De-staining" of FFN200 associated with
447 monoamine vesicular release has been used as a surrogate for neurotransmitter release (Pereira et
448 al., 2016). Consistent with a previous report (Pereira et al., 2016), we found following vehicle
449 (aCSF) application there is a time-dependent and slow de-staining of FFN200 at striatal dopamine
450 terminals (Supplemental Figure 1), suggesting a direct correlation between spontaneous firing
451 activity of dopamine neurons and neurotransmitter release. Manganese increased FFN200 release
452 as measured by increased rate and magnitude of fluorescence de-staining (see supplemental movie
453 1). These data suggest manganese-stimulation of neuronal activity correlates with increased
454 neurotransmitter release (see yellow arrows in Supplemental Figure 1, mean ± SEM, $F_{(1,148)} = 70.2$,
455 †: $p < 0.01$, one-way ANOVA followed by Tukey's test, $n = 4$ slices / group). Additional control
456 experiments were performed when the release of FFN200 is inhibited. Since blockade of
457 dopamine transporter (DAT) decreases firing activity of dopamine neurons (Saha et al., 2014; Lin
458 et al., 2016), theoretically, it should decrease the de-staining rate or even increase the fluorescent
459 punctate due to accumulation of FFN200-filled synaptic vesicles in the terminal regions. As shown
460 in Supplemental Figure 1, treatment with DAT inhibitor nomifensine (5 μM) produced a plateau
461 in the fluorescent signal followed by increased fluorescent levels, suggesting inhibition of
462 neurotransmitter release. These data further support the findings that manganese treatment
463 increases the activity of dopaminergic neurons.
464
465 **Removal of extracellular $Ca^{2+}$ did not prevent manganese stimulation of spontaneous spike**
466 **frequency.** Our observed broad action potentials and slow autonomous pacemaking activities are
467 consistent with typical electrophysiological features in dopamine neurons (Bean, 2007). Numerous
468 studies have shown that slow rhythmic spiking is accompanied by large oscillations in intracellular

469 $Ca^{2+}$ concentrations that are driven by the opening of voltage-dependent $Ca^{2+}$ channels (Guzman
470 et al., 2009; Mercuri et al., 1994; Nedergaard et al., 1993; Puopolo et al., 2007). Therefore, next
471 we measured manganese-regulation of the spontaneous firing activity of dopamine neuron in $Ca^{2+}$–
472 free extracellular solution. Unexpectedly, removal of extracellular $Ca^{2+}$ did not prevent
473 manganese-stimulation of the firing frequency (Figure 3A, C; baseline: 1.3 ± 0.2 Hz vs. manganese
474 in $Ca^{2+}$–free: 6.5 ± 1.1 Hz; $F_{(2,18)} = 20.9$, $p = 0.000002$, one-way ANOVA followed by Tukey's
475 test; $n = 7$ / group). $Ca^{2+}$–free solution containing manganese did not change the membrane
476 potential (Figure 3D), AP half-width (Figure 3E), or CV (Figure 3G); however, it significantly
477 truncated the amplitude of AP (Figure 3F; baseline: 45.4 ± 2.2 mV vs. manganese in $Ca^{2+}$–free:
478 37.9 ± 0.7 mV; $F_{(2,18)} = 16.1$, $p = 0.0001$, one-way ANOVA followed by Tukey's test; $n = 7$ /
479 group). In the absence of manganese, comparison of the firing activity before and after perfusion
480 of a $Ca^{2+}$–free external solution revealed a reduction in the firing frequency (Figure 3C, 0.5 ± 0.03
481 Hz), broadening of AP half-width (Figure 3E: baseline: 1.6 ± 0.08 ms vs $Ca^{2+}$–free: 2.9 ± 0.2 ms,
482 $F_{(2,18)} = 35.9$, $p = 0.0001$, one-way ANOVA followed by Tukey's test; $n = 7$ / group), truncated AP
483 amplitude (Figure 3F, 32.5 ± 2.0 mV, $n = 7$ / group), and an increased CV (Figure 4G, baseline:
484 1.1 ± 0.2 vs $Ca^{2+}$–free: 1.99 ± 0.3, $F_{(2,18)} = 7.3$, $p = 0.004$, one-way ANOVA followed by Tukey's
485 test; $n = 7$ / group). These results suggest that manganese stimulation of neuronal activity it is not
486 dependent on extracellular $Ca^{2+}$ influx into the dopamine neuron.
487
488 **Combined application of $Ca^{2+}$–free external solution and chelation of intracellular $Ca^{2+}$ did**
489 **not prevent manganese-stimulation of firing frequency.** Since excluding extracellular $Ca^{2+}$
490 ($Ca^{2+}$–free external solution) did not decrease the effect of manganese on the spontaneous firing
491 activity of dopamine neurons, AP half-width, amplitude, and CV (Figure 3), we asked whether

492 manganese promotes neuronal activation by increasing intracellular $Ca^{2+}$ concentrations($[Ca^{2+}]_i$)
493 (Tjalkens et al., 2006). To test this, neurons were pretreated with BAPTA-AM (10 mM), a
494 membrane permeable $Ca^{2+}$ chelator, to deplete $[Ca^{2+}]_i$ followed by application of manganese in
495 the presence of $Ca^{2+}$–free external solution. Consistent with previous reports (Benedetti et al., 2011;
496 Torkkeli et al., 2012), BAPTA pretreatment prior to bath application of manganese in $Ca^{2+}$–free
497 external solution (denoted in blue) depolarized the membrane potential (Figure 4D, baseline: -
498 54.9 ± 1.3 mV vs. 100 µM manganese: -49.6 ± 1.9 mV; $F_{(2,27)} = 2.5$, $p = 0.028$, one-way ANOVA
499 followed by Tukey's test; $n = 9$ / group) and broadened the AP half-width (Figure 4B, E baseline:
500 1.37 ± 0.2 ms vs. 100 µM manganese: 2.50 ± 0.3 ms; $F_{(2,24)} = 3.5$, $p = 0.009$, one-way ANOVA
501 followed by Tukey's test; $n = 10$ / group). Interestingly, we found that manganese treatment in
502 $Ca^{2+}$–free external solution (denoted in red) still increased the spontaneous firing activity of the
503 neurons (Figure 4A, C, baseline: 0.9 ± 0.2 Hz vs. 100 µM manganese: 6.9 ± 1.7 Hz, $F_{(2,26)} = 13.2$,
504 $p = 0.003$, one-way ANOVA followed by Tukey's test; $n = 10$ / group) and truncated the amplitude
505 of APs (Figure 4B, F; baseline: 37.5 ± 1.4 mV vs. 100 µM manganese: 29.0 ± 1.7 mV; $F_{(2,24)} =$
506 6.0, $p = 0.001$, one-way ANOVA followed by Tukey's test; $n = 9$ / group). Washout of extracellular
507 manganese in neurons pretreated with BAPTA and recorded in $Ca^{2+}$–free external solution
508 (denoted in green) exhibited a significant decrease in the firing frequency (Figure 4C, 0.4 ± 0.08
509 Hz), a broadening of AP half-width (Figure 4B, E:2.4 ± 0.4 ms, $F_{(2,24)} = 4.3$, $p = 0.029$, one-way
510 ANOVA followed by Tukey's test; $n = 9$ / group), and truncated AP amplitude (Figure 4B, F, 31.7
511 ± 2.1 mV, $F_{(2,24)} = 6.0$, $p = 0.028$, one-way ANOVA followed by Tukey's test; $n = 9$ / group). These
512 results suggest manganese-enhancement of firing frequency of dopamine neurons (Figure 1-3) is
513 not due to the release of $Ca^{2+}$ from intracellular stores.
514

**Manganese does not affect intracellular $Ca^{2+}$ homeostasis in midbrain dopamine neurons.** To directly examine the effect of manganese exposure on $[Ca^{2+}]_i$ in dopamine neurons, we measured $Ca^{2+}$ responses in the midbrain slices from mice conditionally expressing GCaMP6f in dopaminergic neurons. Brain slices were continuously perfused with aCSF containing manganese or N-Methyl-d-aspartate (NMDA) equilibrated with 95% $O_2$-5% $CO_2$. Since NMDA receptors are $Ca^{2+}$-permeable glutamate receptors (Choi, 1987; Wild et al., 2014), 100 μM NMDA was used as a positive control. Representative two-photon $Ca^{2+}$ images are shown in Figure 5, where images for manganese (Figure 5A) or NMDA (Figure 5B) were taken for 10 min after 10 min of baseline imaging. We found manganese exposure (100 μM) did not significantly alter $[Ca^{2+}]_i$ compared to vehicle control. In contrast, 100 μM NMDA markedly increased $[Ca^{2+}]_i$ in the neurons. The relative intensity of two-photon $Ca^{2+}$ signaling over baseline over time is shown in Figure 5C, and supplemental movie 2, and 3. The signal intensity was not affected by manganese administration (black) $[Ca^{2+}]_i$ whereas NMDA (red) robustly increased the GCaMP6f response, especially in neurons with low baseline fluorescence ($F_{(1,592)} = 115.1$, †: $p < 0.001$, one-way ANOVA followed by Tukey's test, *n*: Mn = 10; NMDA = 11). In complement, ratiometric $Ca^{2+}$ imaging using FURA-2 AM in cultured dopamine neurons confirmed the findings that manganese does not affect intracellular $Ca^{2+}$ homeostasis in primary culture midbrain dopamine neurons (Supplemental Figure 2). Collectively, the lack of effect of manganese on $Ca^{2+}$ homeostasis both in midbrain slices and culture is consistent with the notion that the effects of manganese on dopamine neurons are not a result of $Ca^{2+}$ modulation.

**Cadmium blockade of voltage-gated $Ca^{2+}$ channels inhibited manganese-stimulation of spontaneous firing activity of dopamine neurons.** Thus far, above data suggest manganese

538 enhances the spontaneous activity of midbrain dopamine neurons, but rhythmic spiking changes
539 during administration of manganese are unlikely to involve extracellular $Ca^{2+}$ influx or cytosolic
540 $Ca^{2+}$ release from intracellular stores. To further corroborate whether or not manganese augments
541 the spontaneous activity of dopamine neurons through $Ca^{2+}$ channels, we examined the effect of a
542 nonselective $Ca^{2+}$ channel blocker, cadmium ($Cd^{2+}$, 100 μM) on the intrinsic firing behaviors of
543 dopamine neurons following manganese exposure. As shown in Figure 6, nonselective blockade
544 of $Ca^{2+}$ channels by bath application of $Cd^{2+}$ suppressed the spontaneous firing rate of dopamine
545 neurons (Figure 6A). Unexpectedly, we found under this condition, manganese application failed
546 to enhance the firing frequency (Figure 6A, C: $F_{(2,18)} = 8.3$, $p = 0.002$, one-way ANOVA followed
547 by Tukey's test, $n = 7$ group). Treatment with $Cd^{2+}$ alone or the co-administration of $Cd^{2+}$ and
548 manganese did not change the membrane potential (Figure 6D), AP half-width (Figure 6B, E), and
549 AP half-amplitude (Figure 6B, F), but as expected significantly increased the CV (Figure 6G: $F_{(2,18)}$
550 $= 4.6$, $p = 0.024$, one-way ANOVA followed by Tukey's test, $n = 7$ group). These findings suggest
551 that despite observations that manganese-mediated increase in firing activity of dopamine neurons
552 is not dependent on extracellular or intracellular $Ca^{2+}$ flux, it is dependent on $Ca^{2+}$ channels
553 expressed on dopamine neurons.
554
555 The $Ca^{2+}$ current involved in pace-making activity is partly due to L-type currents, which are
556 activated at subthreshold potential which might contribute to tonic firing (Putzier et al., 2009). To
557 investigate the possible role of these channels, we asked whether nifedipine-blockade of L-type
558 $Ca^{2+}$ ($Ca_v1$) channels inhibited manganese-stimulation of spontaneous firing activity of dopamine
559 neurons. As shown in Figure 7, we found nifedipine inhibited manganese-stimulation of
560 spontaneous firing activity. Consistent with the results in Figure 3-4, the firing frequencies were

increased in the presence of manganese and $Ca^{2+}$-free condition. Similar to the $Cd^{2+}$-inhibition of manganese-stimulation of firing activity of dopamine neurons, co-application of nifedipine inhibited the manganese-stimulation of firing activity (Figure 7A, C: $F_{(2,18)} = 44.4$, $p = 0.0006$, one-way ANOVA followed by Tukey's test, $n = 7$ group). Similar to $Cd^{2+}$, the manganese in $Ca^{2+}$–free solution condition or the co-administration of manganese plus nifedipine in $Ca^{2+}$-free solution did not change the membrane potential (Figure 5D) or AP half-width (Figure 5B, E), but both manganese in $Ca^{2+}$–free solution and additional application of nifedipine largely truncated AP amplitudes (Figure 7A, F: $F_{(2,18)} = 11.80$, $p = 0.001$, one-way ANOVA followed by Tukey's test, $n = 7$ group). The co-administration of manganese in $Ca^{2+}$-free manganese and nifedipine significantly increased the CV (Figure 7G: $F_{(2,18)} = 14.11$, $p = 0.0016$, one-way ANOVA followed by Tukey's test, $n = 7$ group). These unexpected results support the interpretation that manganese may influx into the neurons through the nifedipine-sensitive voltage-gated $Ca^{2+}$ channels.

**Single neuron recording revealed manganese competes with $Ca^{2+}$ influx and generates $Ca^{2+}$ channel-like currents.** Because the blockade of voltage-gated $Ca^{2+}$ channels prevented the manganese-mediated increases in the spontaneous firing activity of dopamine neurons independent of the presence of intracellular or extracellular $Ca^{2+}$, we then examined the hypothesis that voltage-gated $Ca^{2+}$ channels on dopamine neurons where directly permeable to extracellular manganese. After replacing external $Ca^{2+}$ with equimolar manganese, we observed manganese induced a $Ca^{2+}$ channel-mediated current, which was evoked by a series of 200 ms depolarizing steps from −60 to +85 mV in 5 mV increments (Figure 8$A_1$). The currents were composed of a rapidly inactivating transient component and a slowly inactivating persistent component. The current–voltage relationship of the manganese current is shown in Figure 8B. The manganese currents were

activated at voltages around 20 mV and peaked at approximately 30 mV. Next, we asked whether the activity of $Ca^{2+}$ channels in midbrain dopamine neurons is affected by these manganese-mediated currents. Since there is little information on whether manganese modulates $Ca^{2+}$ currents in dopamine neurons, we focused on the action of manganese on whole-cell $Ca^{2+}$ currents. Total $Ca^{2+}$ currents (Figure $8A_2$, C) were activated at voltages around 20 mV and peaked at approximately 45 mV. Bath application of 100 μM manganese suppressed the peak amplitude of total $Ca^{2+}$ currents (Figure $8A_3$, C, $^*p < 0.05$, two-tailed Student's *t* tests; $n = 7$ / group). These data suggest in dopamine neurons, manganese might compete with $Ca^{2+}$ influx and generate $Ca^{2+}$ channel-gated-like currents that in turn alter the activity of the neurons. To our knowledge, these are the first reported findings that $Ca^{2+}$ channels may be directly permeable to manganese and may represent a distinct role of manganese in regulating neuronal activity.

**Manganese-enhanced magnetic resonance imaging provides evidence for an $Ca^{2+}$-channel dependent mechanism in the midbrain *in vivo*.** To further examine the manganese interaction with $Ca^{2+}$ channels, we asked whether manganese can influx into the $Ca_v1.2$ and $Ca_v1.3$ expressing cells and whether nifedipine inhibits manganese influx through $Ca_v1$ channels. To examine this hypothesis *in vivo*, we performed manganese enhanced magnetic resonance imaging (MEMRI) in animals pretreated with saline or manganese. I.p. injections of 70 mg/kg manganese has previously been shown to significantly increase manganese levels in the basal ganglia (Dodd et al., 2005), and also is a side-effect of contrast agent for MRI (Poole et al., 2017). Manganese frequently serves as a neuronal contrast agent to enhance functional brain mapping at a higher spatial resolution than typical fMRI studies (Lee et al., 2005). In this study, we utilized MEMRI and $T_1$ mapping to study basal levels of brain activity before and after nifedipine-blockade of voltage-gated $Ca^{2+}$ channels

(Figure 9 and Supplemental Figure 3). A commonly used concentration of nifedipine (15 mg/kg) (Morellini et al., 2017, Giordano et al., 2010) was injected before 30 min of manganese exposure. As expected, we found that $T_1$ relaxation (quantified as $R_1$ or the rate of $T_1$ relaxivity in $s^{-1}$) following manganese treatment exhibited predominantly higher (faster) $R_1$ in ventral tegmental area (VTA) and substantia nigra (SN) compared to other cortical and subcortical regions (Supplemental Figure 3, $F_{(8,72)} = 2.35$, $p = 0.026$, one-way ANOVA followed by Tukey's test, test, $n = 8 - 9$ / group). This reflects a shortening of VTA and SN T1 relaxation time due to the accumulation of the paramagnetic manganese. Importantly, and consistent with single neuron recordings (Figure 6, 7, and 8), we observed that nifedipine-blockade of L-type $Ca^{2+}$ channels reduced $T_1$ shortening effects of manganese in dopaminergic midbrain regions (Fig 9, VTA: $t_{(15)} = -2.2$, $p = 0.04$, two-tailed Student's t tests; Sn: $t_{(15)} = -2.7$, $p = 0.015$, two-tailed Student's t tests; $n = 8 - 9$ / group). This was observed as a slower rate $R_1$ in the nifedipine/manganese group relative to manganese only. Therefore, both *in vitro* (single neurons recording) and *in vivo* studies suggest that nifedipine decreases manganese-stimulation of neuronal activity and its accumulation in the multiple brain regions including the dopamine neuron enriched midbrain.

**Manganese influxes into $Ca_v1.2$ and $Ca_v1.3$ expressing cells in a nifedipine-dependent manner.** Our data so far supports the interpretation that manganese may influx via nifedipine-sensitive $Ca^{2+}$ channels. To examine this idea directly in a reduced system, HEK cells were transiently transfected with either a control empty vector or $Ca_v1.2$ or $Ca_v1.3$ cDNA. Western blot analysis confirmed the greater expression of $Ca_v1.2$ or $Ca_v1.3$ in the transfected cells (Figure 10A). Overexpression of $Ca_v1.2$ increased the uptake of $^{54}Mn$ at 5 and 15 min after the addition of $^{54}Mn$, while there was no difference observed between the $Ca_v1.3$ expressing and control cells (Figure

10B). Uptake of $^{54}Mn$ by HEK cells overexpressing $Ca_v1.2$ was inhibited by pretreating with nifedipine (Figure 10C). These findings support the interpretation that manganese regulates dopamine neuronal activity and manganese influx via a nifedipine-sensitive $Ca_v1.2$-channel-mediated mechanism.

**In silico modeling support the possibility that manganese can interact with the $Ca^{2+}$ binding site in the $Ca_v1$ channel.** Because the crystal structure for $Ca_v1.2$ is not available, Cav1.1 was used for the homology modeling studies to investigate whether the putative structure of $Ca_v1.2$ could informs us about the manganese cation transport. First, the available electron microscopy structure for the homologous $Ca_v1.1$ channel was used to build a homology model using the SWISS-MODEL program (Figure 11) (Waterhouse et al., 2018). The helical regions of the mouse $Ca_v1.1$ structure (Wu et al., 2016) and the helical regions for the $Ca_v1.2$ model were compared by protein BLAST (Altschul et al., 1990) and found to be 72% identical and 81% similar. Further, when all amino acids within 7 Å of the bound $Ca^{2+}$ atom found in the $Ca_v1.1$ structure were selected and compared to amino acids in the model structure for $Ca_v1.2$, we found 100% identity in this region, including the carboxylate ligands for the $Ca^{2+}$ atom. We conclude the $Ca_v1.2$ channel has an extremely similar structure and presumably cation-binding capability when compared with $Ca_v1.1$. Because the ionic radius of $Mn^{2+}$ is smaller than for $Ca^{2+}$ (Persson, 2010), it should be adequately accommodated by the channel. Taken together, the structural features of the $Ca_v1.2$ channel and our experimental findings argue for the possibility of the $Ca_v1.2$ channel conducting a manganese ion. While these data collectively suggest manganese produces a $Ca^{2+}$ channel-mediated current in dopamine neurons, which increases rhythmic firing activity of dopamine neurons, the connection between manganese-mediated current and increased firing activity of

dopamine neurons remain unclear. The next set of experiments are designed to determine the mechanism.

**Blockade of large-conductance $Ca^{2+}$-activated potassium (BK) channels decreased the spontaneous firing activity and prevented manganese-stimulation of firing frequency.** Previously, we have shown that paxilline-blockade of BK channels reduces the spontaneous firing activity, broadens the width and enhances the amplitude of action potentials in midbrain dopamine neurons (Lin et al., 2016). Since Mn increased the firing frequency, decrease the width and the amplitude of action potentials (Figure 1), we postulated that manganese-stimulation of the firing frequency, narrowing of action potential width and reduction of action potential amplitude might be due to BK channel activation. Consistent with our previous reports, paxilline suppressed the firing frequency of midbrain dopamine neurons (Figure 12A, B). Pre-treatment with paxilline abolished the manganese-induced increase in firing frequency (Figure 12A, C: baseline: 1.5 ± 0.2 Hz vs. Mn + paxilline: 0.51 ± 0.1 Hz; $F_{(2,20)} = 11.2$, $p = 0.0005$, one-way ANOVA followed by Tukey's test; $n = 8$ / group) and inhibited manganese's modulation of action potential amplitude (Figure 12A, F). Comparison of the firing frequency after treatment with paxilline alone or paxilline + manganese treatment revealed a further reduction in the firing frequency (Figure 12C; paxilline: 0.81 ± 0.1 Hz). Consistent with our previous report (Lin et a., 2016), blockade of BK channels depolarized membrane potential (Figure 12D; Baseline: -45.1 ± 1.6 mV vs paxilline: -40.1 ± 1.8 mV; $F_{(2,21)} = 3.5$, $p = 0.04$, one-way ANOVA followed by Tukey's test; $n = 8$ / group), broadened AP half-width (Figure 12B, E: baseline: 1.3 ± 0.1 ms vs. paxilline: 1.8 ± 0.2 ms; ; $F_{(2,21)} = 5.9$, $p = 0.009$, one-way ANOVA followed by Tukey's test; $n = 8$ / group), increased action potential amplitude (Figure 12B, F; baseline: 28.1 ± 1.6 mV vs. paxilline: 32.6 ± 1.1 mV; $F_{(2,21)}$

676 = 6.6, $p = 0.005$, one-way ANOVA followed by Tukey's test; $n = 8$ / group) and increased the CV
677 (Figure 12G; baseline: 1.8 ± 0.2 vs. paxilline: 2.8 ± 0.3; $F_{(2,21)} = 2.8$, $p = 0.015$, one-way ANOVA
678 followed by Tukey's test; $n = 8$ / group). After pretreatment with paxilline, we found manganese
679 did not reverse paxilline-induced membrane depolarization (Figure 12D), but it did diminish the
680 effects of paxilline on the action potential half-width (Figure 12E), amplitude (Figure 12F) and
681 CV (Figure 12G). These results suggest that the manganese-stimulation of spontaneous spike
682 activity of dopamine neurons is possibly due to BK channels activation.
683
684 **Manganese increases membrane expression of BK-α subunits.** The BK-α subunit is the pore-
685 forming unit of the BK channel (Knaus et al., 1994). There is a direct relationship between BK
686 channel regulation of neuronal excitability and the level of BK-α subunits at the surface membrane
687 (Shruti et al., 2012; Chen et al., 2013; Cox et al., 2014). Since blockade of BK channels abolished
688 the effect of manganese-stimulation of the spontaneous firing frequency of dopamine neurons, we
689 examined the possibility that manganese-mediated enhancement of neuronal excitability is due to
690 increased BK-α subunit levels at the plasma membrane. To test this, we used TIRF microscopy to
691 monitor fluorescently-tagged BK channel trafficking. The TIRF profile of GFP-α subunits was
692 examined in HEK293 cells expressing GFP-α subunits in the presence or absence of 100 μM
693 manganese. As shown in Figure 13 and supplemental movie 4, the GFP-α subunits' fluorescence
694 signal at the membrane remained stable in the vehicle (external solution)-treated control group.
695 The TIRF profile of GFP-α subunits was markedly increased following manganese treatment
696 ($F_{(1,164)} = 163.8$, †: $p < 0.01$, one-way ANOVA followed by Tukey's test, $n$: baseline = 7; Mn = 8).
697 Because TIRF microscopy detects fluorophores at or near the plasma membrane, these results
698 indicate that manganese's stimulation of neuronal excitability is, in part, due to manganese-

699 induced increases in surface BK channel expression and thus activity. To test this possibility, we
700 used excised inside-out patches to record currents in response to test voltage steps. Figure 14 shows
701 representative BK currents in response to test voltage steps in the absence or presence of
702 manganese. The I–V curves of these recordings demonstrate Mn significantly increased peak
703 amplitude of BK currents ($^{*}p < 0.05$, two-tailed Student's *t* tests, $n = 6$ / group). Taken together,
704 these results suggest manganese enhances BK channel activity that we have previously shown
705 increases firing activity of dopamine neurons (Lin 2016).
706
707
708 **Discussion**
709
710 Prolonged exposure to low levels of manganese or single large exposure results in its accumulation
711 in multiple brain regions leading to dysfunction of central nervous system and an extrapyramidal
712 motor disorder referred to as manganism (Aschner et al., 2009). In this study, we used multiple
713 complementary approaches to examine the manganese-regulation of dopaminergic excitability and
714 to determine the potential mechanisms involved. We found manganese increased the spontaneous
715 firing activity of dopamine neurons, decreased the amplitude and half-width of action potentials,
716 and reduced the variation of interspike interval. Unexpectedly, neither the removal of extracellular
717 $Ca^{2+}$ and/or the chelation of intracellular $Ca^{2+}$ modulated the manganese-stimulation of
718 spontaneous firing frequency of dopamine neurons. Live cell two-photon imaging of GCaMP6f
719 expressing dopamine neurons support the electrophysiology data showing no change in
720 intracellular $Ca^{2+}$ levels after manganese application. In contrast, we found manganese-regulation
721 of dopamine neurons was blocked by cadmium, a nonselective $Ca^{2+}$ channel blocker or by

722 nifedipine, an L-type $Ca^{2+}$ channel blocker, suggesting manganese can potentially influx through
723 voltage-gated $Ca^{2+}$ channels. Furthermore, we identified a $Ca^{2+}$ channel-mediated manganese
724 current that reduced voltage-gated $Ca^{2+}$ currents, supporting the idea that manganese may compete
725 with $Ca^{2+}$ influx, leading to activation of BK channels and increased spontaneous firing activity of
726 dopamine neurons.
727
728 **Manganese competes with $Ca^{2+}$ entry through voltage-gated $Ca^{2+}$ channels to enhance**
729 **excitability of dopamine neurons.** The action potential of dopamine neurons is slow and broad,
730 which maximizes $Ca^{2+}$ entry and promotes slow rhythmic activity (Bean, 2007). The slow,
731 rhythmic activity (2–10 Hz) in these neurons is autonomously generated and accompanied by slow
732 oscillations in intracellular $Ca^{2+}$ concentration that are triggered by the opening of plasma
733 membrane $Ca_v1$ ($Ca_v1.2$, $Ca_v1.3$) $Ca^{2+}$ channels and release of $Ca^{2+}$ from intracellular, endoplasmic
734 reticulum stores (Guzman et al., 2009; Morikawa and Paladini, 2011; Nedergaard et al., 1993;
735 Puopolo et al., 2007). Thus, we tested the hypothesis that manganese increases $Ca^{2+}$ entry into the
736 neuron and/or releases $Ca^{2+}$ from intracellular $Ca^{2+}$ stores. Unexpectedly, our data support neither
737 of these possibilities. We found performing the experiments in either extracellular $Ca^{2+}$-free
738 condition or chelation of intracellular $Ca^{2+}$ did not impair manganese-stimulation of firing
739 frequency or reduction of action potential amplitude. Consistently, live cell two-photon $Ca^{2+}$
740 imaging showed manganese did not alter intracellular $Ca^{2+}$ concentration in the midbrain
741 dopamine neurons. Thus, although manganese has been previously shown to regulate $Ca^{2+}$
742 homeostasis in astrocytes (Xu et al., 2009), this effect is not present in dopamine neurons. Previous
743 studies suggest manganese can enter cells through a number of transporters (Gunshin, 1997;
744 Lockman et al., 2001; Crossgrove and Yokel, 2005; Goytain et al., 2008; Itoh et al., 2008; Gunter

et al., 2013). In addition, as a divalent cation, manganese may potentially target $Ca^{2+}$ channels, which are also permeant to other divalent cations such as barium (Bourinet et al., 1996). Therefore, if manganese competes with $Ca^{2+}$ entry at the level of voltage-gated $Ca^{2+}$ channels, then a nonselective $Ca^{2+}$ channel blocker such as cadmium ($Cd^{2+}$) or a L-type $Ca^{2+}$ channel nifedipine should block the effect of manganese on the firing frequency of dopamine neurons and action potential morphology. As shown in Figure 6 and 7, both of $Cd^{2+}$ and nifedipine suppressed manganese–stimulation of spontaneous firing activities, which is consistent with recent reports showing dihydropyridine L-type channel inhibitors slow pacemaker activity of dopamine neurons at submicromolar concentrations (Nedergaard et al., 1993; Puopolo et al., 2007).

**Blockade of L-type $Ca^{2+}$ (Cav1) channels decreases manganese influx.** Since the 1980s, manganese has been used as a tool to increase the signal to noise ratio in magnetic resonance imaging (MRI) (Lauterbur et al., 1980). Consistent with previous reports (Aoki et al., 2004; Lee et al., 2005), following systemic manganese administration, manganese is accumulated in multiple brain regions including dopaminergic neuron enriched brain regions such as substantia nigra and ventral tegmental area (Figure 9 and Supplemental Figure 3). Here we found, nifedipine-blockade of L-type $Ca^{2+}$ channels decreased manganese accumulation in several brain regions as well as manganese uptake in the $Ca_v1.2$ expressing HEK cells. These data support the interpretation that manganese might be permeable through the $Ca^{2+}$ channels. Consistent with this idea, the chemical properties of aqueous $Ca^{2+}$ and $Mn^{2+}$ ions and the smaller ionic radius of $Mn^{2+}$ than for $Ca^{2+}$ also support the hypothesis that manganese might be accommodated by the $Ca_v1$ channels. While the crystal structure of $Ca_v1.2$ is yet to be determined, *in silico* analyses of the homology model of the helical regions of the mouse $Ca_v1.1$ structure and the helical regions for the $Ca_v1.2$ were found to

768 be 72% identical and 81% similar for $Ca_v1.2$; therefore, it is possible that $Mn^{2+}$ enters Cav
769 expressing cells. Whether manganese is permeable to other $Ca^{2+}$ channels in dopamine or other
770 neuronal types requires further examination.
771
772 Manganese influx through L-type $Ca^{2+}$ channels was further supported by our manganese
773 enhanced magnetic resonance imaging (MEMRI) data (Figure 9). It should be noted that both
774 neuronal and glial cells express $Ca_v1$ channels and therefore the MEMRI and the nifedipine-
775 inhibition of this response reported in our studies do not distinguish the cell type. While the effect
776 of manganese on $Ca_v1.2$ is consistent across other CNS cell types requires further investigation,
777 our observations of manganese accumulation in the dopamine enriched brain region and *in vitro*
778 studies on the effects of manganese on dopaminergic neurons could establish a biological basis for
779 movement disorders associated with manganism, which typically include symptoms related to
780 dysregulation of the dopaminergic system. Furthermore, although the MEMRI data suggest acute
781 manganese exposure can be detected in multiple brain regions, dopaminergic brains regions,
782 specifically the VTA and SN, displayed a greater enhancement of MRI signal by manganese
783 compared to other brain regions observed in this study. Overall, we found that blockade of $Ca_v1.2$
784 can decrease manganese regulation of dopamine neuron activity and its accumulation in the brain.
785
786 **Manganese increases membrane expression of BK channels α-subunit leading to enhanced**
787 **BK channels activity.** Structurally, BK channel complexes contain the pore-forming α subunit
788 (four α subunits form the channel pore) and the regulatory β subunits (Knaus et al., 1994; Brenner
789 et al., 2000; Lu et al., 2006). The intrinsic gating properties of BK channels are dynamically
790 modulated by various kinases (White et al., 1991, Weiger et al., 2002) that regulate BK channels

791 trafficking to the membrane (Chae and Dryer, 2005, Toro et al., 2006). Recently, we have shown
792 that PKC activation decreases membrane expression of GFP-α subunits of BK channels (Lin et al.,
793 2016). These data combined with reports showing manganese-activation of protein kinase delta
794 triggers apoptosis in dopaminergic neurons (Kitazawa et al., 2005), led us to ask whether Mn
795 increases GFP-α subunit membrane expression. We found manganese enhanced surface trafficking
796 of BK channels (Fig 13) and increased BK channels activity (Fig 14). These data collectively
797 describe a cellular mechanism for the paxilline-blockade of Mn-stimulated increases in firing
798 frequency as well as its effect on the action potential morphology. Future studies will determine
799 the PKC subtype/s involved in Mn-induced trafficking of GFP-α subunit of BK channels and the
800 potential involvement of other BK channels subunits such as regulatory β subunits. Collectively,
801 these findings reveal the cellular mechanism for manganese-regulation of dopamine neurons and
802 reveal a unique therapeutic target to attenuate the untoward consequence of manganese exposure.
803

804 **Acknowledgements**

805 This study was supported by DA026947, NS071122, OD020026, DA026947S1, DA043895

806 We are very grateful to Dr. Gregory Hockerman for providing plasmids for $Ca_v$1.2-GFP and
807 $Ca_v$1.3-GFP, Dr. Richard B. Silverman for providing HEK 293 cells stably expressing Cav1.2 or
808 1.3 and Dr. Robert Brenner for providing HEK293 cells stably expressing GFP-BK-α subunits.

809

810 **Figure Legends**

811

812 **Figure 1- Manganese increases the spontaneous firing activity of dopamine neurons.** Top:
813 representative recording showing the dose-dependent effect of $Mn^{2+}$ on the spontaneous firing
814 activity of dopamine neurons and firing rate following washout period. Bottom: Histogram of
815 firing frequency obtained from above trace.
816
817 **Figure 2- Analysis of spontaneous firing activity and properties of action potential following**
818 **manganese exposure.** ***A,*** Representative action potential trace before (baseline, black trace) and
819 after bath application of 100 μM $Mn^{2+}$ (red trace). ***B,*** Dose-response relationships of the
820 spontaneous firing frequency of dopamine neurons following $Mn^{2+}$ exposure. A $EC_{50}$ of 80.2 μM
821 was obtained by fitting the dose-dependent curve using a Hill equation. **C,** $Mn^{2+}$ did not
822 significantly change membrane potential. ***D,*** $Mn^{2+}$ suppressed the amplitude of action potential (as
823 measured as the half amplitude) at all concentrations examined (baseline: 37.2 ± 1.1 mV; 10 μM
824 manganese: 31.1 ± 1.1 mV; $t_{(15)} = 3.6$, p = 0.03, two-tailed Student's t tests; $n = 11$ vs 6). ***E,*** $Mn^{2+}$
825 did not change the half-width of action potential at 10-50 μM, but it significantly narrowed the
826 half-width at 100 μM (baseline: 1.5 ± 0.1 ms; 100 μM manganese: 1.15 ± 0.1 ms; $t_{(15)} = 2.2$, p =
827 0.04, two-tailed Student's t tests; $n = 10$ vs. 7). ***F,*** $Mn^{2+}$ dose-dependently decreased the coefficient-
828 of-variation of interspike intervals (baseline: 1.2 ± 0.1; 200 μM manganese: 0.7 ± 0.1; $t_{(22)} = 3.4$,
829 p = 0.003, two-tailed Student's t tests; $n = 11$ vs 13).
830
831 **Figure 3- Manganese stimulation of firing activity of dopamine neurons is not dependent on**
832 **extracellular $Ca^{2+}$.** ***A,*** Top: representative spontaneous spike activities of a neuron exposed to
833 $Mn^{2+}$ in a $Ca^{2+}$-free extracellular solution. Middle: histogram of firing frequency obtained from
834 the above trace showing $Mn^{2+}$ increased firing frequency. ***B,*** Superimposed representative single

action potential traces shown in A, baseline (black trace), $Mn^{2+}$ + $Ca^{2+}$-free solution (red trace), and $Ca^{2+}$-free solution only (green trace). ***C,*** In $Ca^{2+}$-free solution, $Mn^{2+}$ increased spontaneous firing rate. $Mn^{2+}$ washout in $Ca^{2+}$-free conditions revealed a reduction of firing rate (baseline: 1.3 ± 0.2 Hz vs. manganese in $Ca^{2+}$ – free: 6.5 ± 1.1 Hz; $F_{(2,18)} = 20.9$, $p = 0.000002$, one-way ANOVA followed by Tukey's test; $n$ = 7 / group). ***D,*** $Mn^{2+}$ and $Ca^{2+}$-free extracellular solution did not change membrane potential. ***E,*** Half-width measured at half-maximal voltage of action potential was not different between baseline and $Mn^{2+}$ application, but it was significantly broadened in $Ca^{2+}$-free condition as compared to baseline (baseline: 1.6 ± 0.08 ms vs $Ca^{2+}$ – free: 2.9 ± 0.2 ms, $F_{(2,18)} = 35.9$, $p = 0.0001$, one-way ANOVA followed by Tukey's test; $n = 7$ / group). ***F,*** Both $Ca^{2+}$-free only and $Mn^{2+}$ plus $Ca^{2+}$-free condition significantly depressed the amplitude of action potential (baseline: 45.4 ± 2.2 mV vs. manganese in $Ca^{2+}$ – free: 37.9 ± 0.7 mV; $F_{(2,18)} = 16.1$, $p$ = 0.0001, one-way ANOVA followed by Tukey's test; $n = 7$ / group). ***G,*** The coefficients of variation of the interspike intervals was not different between baseline and Mn plus $Ca^{2+}$-free solution (baseline: 1.1 ± 0.2 vs $Ca^{2+}$ – free: 1.99 ± 0.3, $F_{(2,18)} = 7.3$, $p = 0.004$, one-way ANOVA followed by Tukey's test; $n$ = 7 / group). *p < 0.05; **p < 0.01.

**Figure 4- Manganese increases firing rate in the combined absence of extracellular and intracellular $Ca^2$.** ***A,*** Top: representative trace of spontaneous spike activity following $Mn^{2+}$ exposure in an $Ca^{2+}$-free extracellular solution and an intracellular solution containing the $Ca^{2+}$ chelator BAPTA (10 mM). Bottom: histogram of firing frequency obtained from above trace showing $Mn^{2+}$ increased firing frequency. ***B,*** Superimposed representative single action potential traces are shown in A: baseline (black trace), 100 μM $Mn^{2+}$ + $Ca^{2+}$-free + BAPTA (red trace) and $Ca^{2+}$-free plus BAPTA-AM (green trace). ***C,*** $Mn^{2+}$ increased firing rate even in the combined

absence of extracellular and intracellular $Ca^{2+}$; after $Mn^{2+}$ washout, the firing rate decreased under $Ca^{2+}$-free conditions (baseline: 0.9 ± 0.2 Hz vs. 100 µM manganese: 6.9 ± 1.7 Hz, $F_{(2,26)} = 13.2$, $p = 0.003$, one-way ANOVA followed by Tukey's test; $n = 10$ / group). ***D,*** The combination of extracellular $Ca^{2+}$-free plus $Mn^{2+}$ and intracellular BAPTA containing solution depolarized the membrane potential. After $Mn^{2+}$ washout the membrane potential returned to the baseline level ($Ca^{2+}$-free conditions) (baseline: -54.9 ± 1.3 mV vs. 100 µM manganese: -49.6 ± 1.9 mV; $F_{(2,27)} = 2.5$, $p = 0.028$, one-way ANOVA followed by Tukey's test; $n = 9$ / group). ***E,*** The half-width was measured at the half-maximal voltage of APs. The half-width was broadened significantly in the combination of extracellular $Ca^{2+}$-free + intracellular BAPTA containing solution in the absence or presence of $Mn^{2+}$ (baseline: 1.37 ± 0.2 ms vs. 100 µM manganese: 2.50 ± 0.3 ms; $F_{(2,24)} = 3.5$, $p = 0.009$, one-way ANOVA followed by Tukey's test; $n = 10$ / group). ***F,*** Half-amplitude of action potential was significantly depressed in the combination of extracellular $Ca^{2+}$-free and intracellular BAPTA contained solution in the absence or presence of $Mn^{2+}$ (baseline: 37.5 ± 1.4 mV vs. 100 µM manganese: 29.0 ± 1.7 mV; $F_{(2,24)} = 6.0$, $p = 0.001$, one-way ANOVA followed by Tukey's test; $n = 9$ / group). ***G,*** The coefficients of variation of the interspike intervals were not significantly different amongst the experimental groups. *p < 0.05; **p < 0.01, n = 9 - 10 per group.

**Figure 5- Manganese does not alter intracellular $Ca^{2+}$ homeostasis**. ***A, B,*** Representative two-photon images of GCaMP6f fluorescent neurons in mouse midbrain slices following 100 µM $Mn^{2+}$ or NMDA treatments. ***C,*** Analyses of relative fluorescence intensities of GCaMP6 neurons following 100 µM $Mn^{2+}$ or NMDA ($F_{(1,592)} = 115.1$, †: $p < 0.001$, one-way ANOVA followed by Tukey's test, *n*: Mn = 10 frame (71 neurons) NMDA = 11 frame (50 neurons) from 3 independent experiments). Scale bar: 50 µm. †: p < 0.001.

**Figure 6- Cadmium blockade of voltage-gated $Ca^{2+}$ channels inhibited manganese-stimulation of spontaneous firing activity of dopamine neurons**. ***A,*** Top: representative spontaneous spike activity of a dopamine neuron before and after exposure to cadmium ($Cd^{2+}$ a nonselective voltage-gated $Ca^{2+}$ channel blocker) and $Cd^{2+}$ + $Mn^{2+}$. $Cd^{2+}$-blockade of voltage-gated $Ca^{2+}$ channels inhibited $Mn^{2+}$-stimulation of spontaneous firing activity. Bottom: histogram of firing frequency from above trace showing firing frequencies were lowered in $Cd^{2+}$ only condition and following or $Cd^{2+}$ plus $Mn^{2+}$, but return to baseline after washout. ***B,*** Superimposed representative single action potential traces shown in A: baseline (black trace), 100 µM $Cd^{2+}$ (green trace), 100 µM $Mn^{2+}$ + $Cd^{2+}$ (red trace), and washout (blue trace). ***C,*** Spontaneous firing rate significantly decreased following application of $Cd^{2+}$ or $Cd^{2+}$ plus $Mn^{2+}$ ($F_{(2,18)} = 8.3$, $p = 0.002$, one-way ANOVA followed by Tukey's test, $n = 7$ / group). ***D,*** Application of $Cd^{2+}$ or $Cd^{2+}$ plus $Mn^{2+}$ did not change the membrane potential. ***E,*** Half-width was measured at half-maximal voltage of action potential; there was no change in the half-width of, $Cd^{2+}$ and $Cd^{2+}$ plus $Mn^{2+}$ experimental groups. ***F,*** $Cd^{2+}$ or $Cd^{2+}$ plus $Mn^{2+}$ treatments did not change the amplitude of action potential. ***G,*** Both $Cd^{2+}$ and $Cd^{2+}$ plus $Mn^{2+}$ treatments increased the coefficients of variation of the interspike interval ($F_{(2,18)} = 4.6$, $p = 0.024$, one-way ANOVA followed by Tukey's test, $n = 7$ / group). *p < 0.05; **p < 0.01.

**Figure 7- Blockade of L-type $Ca^{2+}$ channels inhibited manganese-stimulation of spontaneous firing activity of dopamine neurons**. ***A,*** Top: representative spontaneous spike activity of a dopamine neuron before and after exposure to $Mn^{2+}$ plus $Ca^{2+}$-free and nifedipine, an L-type $Ca^{2+}$ channel blocker. Nifedipine-blockade of voltage-gated $Ca^{2+}$ channels inhibited $Mn^{2+}$-stimulation

of spontaneous firing activity. Bottom: histogram of firing frequency from above trace showing firing frequencies were increased in combination of $Mn^{2+}$ and $Ca^{2+}$-free, lowered in additionally added nifedipine, but return to baseline after washout. ***B,*** Superimposed representative single action potential traces shown in A: baseline (black trace), $Mn^{2+}$+ $Ca^{2+}$-free (red trace), $Mn^{2+}$+ $Ca^{2+}$-free + nifedipine (green trace), and washout (blue trace). ***C,*** Mn increased firing rate even in the combination of $Mn^{2+}$ and $Ca^{2+}$-free. Additional application of nifedipine significantly reduced firing rate ($F_{(2,18)} = 44.4$, $p = 0.0006$, one-way ANOVA followed by Tukey's test, $n = 7$ / group). ***D,*** Application of $Mn^{2+}$+ $Ca^{2+}$-free or further administrated nifedipine did not change the membrane potential. ***E,*** Half-width was measured at half-maximal voltage of action potential; there was no change in the half-width of, $Mn^{2+}$+ $Ca^{2+}$-free and additional plus nifedipine experimental groups. ***F,*** Both $Mn^{2+}$ plus $Ca^{2+}$-free and further added nifedipine condition significantly depressed the amplitude of action potential ($F_{(2,18)} = 11.80$, $p = 0.001$, one-way ANOVA followed by Tukey's test, $n = 7$ / group). ***G,*** $Mn^{2+}$ plus $Ca^{2+}$-free and additional application of nifedipine increased the coefficients of variation of the interspike interval ($F_{(2,18)} = 14.11$, $p = 0.0016$, one-way ANOVA followed by Tukey's test, $n = 7$ / group). **p < 0.01.

**Figure 8. Manganese reduced voltage-gated $Ca^{2+}$ currents.** ***A,*** Representative traces of inward currents in response to voltage steps (5 mV, 250 ms) from -60 mV to +85 mV in a bath solution containing 0.5 μM TTX, 35 mM TEA and 1mM CsCl. ***A1***, Inward currents evoked by voltage steps during application of extracellular $Ca^{2+}$-free plus 2mM $Mn^{2+}$ solution. ***A2***, Inward currents evoked by voltage steps in the presence of 2 mM $Ca^{2+}$. ***A3***, Inward currents evoked by voltage steps in the presence of 2 mM $Ca^{2+}$ plus 100 mM $Mn^{2+}$. ***B,*** Plot shows the current-voltage relationship (I–V curves) induced by $Mn^{2+}$. ***C,*** Plot shows current-voltage relationships (I–V curves) of peak voltage-

gated $Ca^{2+}$ current density in dopamine neurons at baseline (black squares) and following $Mn^{2+}$ exposure (blue squares), ($^{*}p < 0.05$, two-tailed Student's *t* tests; $n = 7$ / group).

**Figure 9. Manganese enhanced magnetic resonance imaging (MEMRI) provides evidence of an *in vivo* $Ca^{2+}$-channel dependent mechanism involved in midbrain manganese accumulation.** $R_1$ ($1/T_1$) maps. The top figure displays the location of the ventral tegmental area (VTA) and substantia nigra (SN). The middle figure displays a custom template from all controls and experimental groups (nifedipine administered rats). The bottom figure displays the average $R_1$ map of both cohorts. Maps display values up to 2 $s^{-1}$ with yellow representing large values (~2 s^-1) and red representing low values (~ 0). The control group shows a small number of voxels of $R_1$ larger within the threshold showing less $Mn^{2+}$ infiltration in the midbrain. ***A₁*,** Mouse brain atlas-based segmentation of the VTA and SN. ***A₂*,** Template brain for Mn alone or with nifedipine treatment that were aligned with mouse brain atlas. ***A₃*,** Parametric maps of $T_1$ relaxation rate ($R_1$ in $msec^{-1}$) show that calcium channel blockade with nifedipine treatment reduces $R_1$ in midbrain and surrounding areas. Scale bar indicates intensity of $R_1$. ***B*,** Nifedipine reduces $T_1$ relaxation rate ($R_1$) in VTA and SN (VTA: $t_{(15)} = -2.2$, p = 0.04, two-tailed Student's t tests; Sn: $t_{(15)} = -2.7$, p = 0.015, two-tailed Student's t tests; $n = 8 – 9$ / group). ***C*,** A greater $Mn^{2+}$ accumulation produces faster rates of $T_1$ relaxation ($R_1$) in VTA and SN than in other cortical and subcortical nuclei ($F_{(9,72)} = 3.96$, $p < 0.001$, one-way ANOVA followed by Tukey's test, $n = 8 – 9$ / group). **p < 0.01.

**Figure 10. $^{54}Mn$ uptake is greater in $Ca_v1.2$ overexpressing HEK293 cells.** ***A*,** Representative western blot analysis is showing the expression of $Ca_v1.2$ and $Ca_v1.3$ in cells transiently-transfected to overexpress $Ca_v1.2$ and $Ca_v1.3$. ***B*,** Greater $^{54}Mn$ uptake is shown in $Ca_v1.2$

overexpressing cells at the indicated time points. ***C,*** Nifepidine inhibits $^{54}$Mn uptake at 15 minutes in $Ca_v1.2$ overexpressing cells. (One-way ANOVA followed by Tukey's test, n = 3 / group). *p<0.05)

**Figure 11. Superposition of msCa$_v$1.1 Ca binding site structure with the msCa$_v$1.2 model.** The $Ca^{2+}$ ion (green) as located in the msCa$_v$1.1 structure (tan color backbone) (PDB ID 5GJW). The homology model structure for Ca$_v$1.2 alpha chain is shown in the blue color backbone.

**Figure 12- Blockade of BK channels inhibited Manganese-stimulation of the spontaneous firing activity in dopamine neurons.** ***A,*** Top: representative spontaneous firing activities of a dopamine neuron exposed to paxilline followed by Mn treatment. Firing rate returns to baseline after washout with artificial cerebral spinal fluid (aCSF) solution. Bottom: Rate histogram of above trace. ***B,*** Superimposed traces of representative single action potential shown in A: baseline (black trace), paxilline (green trace), Mn (red trace) and washout (blue trace). ***C,*** Paxilline reduced the spontaneous firing rate; Mn treatment did not attenuate the paxilline-induced reduction of firing activity. ***D,*** Paxilline and concomitant Mn + paxilline applications significantly depolarized the membrane potential. ***E,*** Half-width is measured at half-maximal voltage of action potential. The half-width was broadened after paxilline application, but returned to baseline after co-administration of Mn and paxillin. ***F,*** Paxilline increased the amplitude of action potential, but diminished the effect of Mn on the action potential amplitude. ***G,*** Blockade of BK channels exhibited larger coefficients of variation of the interspike interval. *p < 0.05; **p < 0.01, n = 8 per group.

973 **Figure 13- Membrane localization of BK GFP-α subunit is increased followed manganese**
974 **exposure.** ***A,*** Representative TIRF microscopy images of GFP-α subunit following vehicle or 100
975 μM $Mn^{2+}$ treatments. ***B,*** Analyses of relative fluorescence intensities at the surface membrane
976 following vehicle or 100 μM $Mn^{2+}$. Scale bar: 20 μm. †: $p < 0.01$.
977
978 **Figure 14- Manganese increases BK currents.** ***A,*** Representative traces of outward currents in
979 response to voltage steps (5 mV, 250 ms) from -60 mV to +85 mV in a bath solution containing
980 0.5 μM TTX, 35 mM TEA and 1mM CsCl. ***A***, In cells expressing BK-α subunits, families of
981 outward currents were evoked by voltage steps from −60 to +85 mV for 250 ms with 5 mV
982 increments every 5 s from the holding potential of −70 mV, before (A) and after (B) Mn
983 administration. ***C,*** shows peak current-voltage relationships (I–V curves) before (baseline) and
984 after Mn application. *$p < 0.05$.
985
986 **Supplemental Figure. 1**. **$Mn^{2+}$ induces release of FFN200 from dorsal striatum.** ***A***. Time lapse
987 images of a striatal slice loaded with FFN200 following nomifensine (A top panel) or 100 μM
988 $Mn^{2+}$ treatments (A bottom panel). $Mn^{2+}$ treatment decreased FFN200 puncta intensities (yellow
989 arrows). ***B***. ***C***. Quantification of FFN200 puncta fluorescence normalized to the averaged intensity
990 of first 60sec for each experimental condition. Scale bar: 10 μm. †: $p < 0.01$.
991
992 **Supplemental Figure 2- Mn does not increase intracellular calcium**. Ratiometric analyses were
993 performed on Fura-2-loaded dopamine neurons. ***A,*** Representative pseudo color images indicating
994 the 340/380 ratio via a visible spectrum heat map (violet – minimum $Ca^{2+}$; red – maximum $Ca^{2+}$).
995 Left panel shows representative 340/380 ratio images before and after drug or vehicle application,

996 right panel shows identical view-fields 30-seconds after vehicle (top), 100 μM Mn (middle) and
997 20mM caffeine (bottom). ***B,*** Mean fluorescence intensities for each condition (normalized to the
998 initial 30 s intensity). Data are plotted in 1.5 s interval for vehicle (black squares), $Mn^{2+}$ (red
999 squares), caffeine (blue squares). Scale bar: 20 μm. †: $p < 0.01$.
1000
1001
1002 **Supplemental Figure 3- $Ca^{2+}$ channel blockade using nifedipine reduces the effects of $Mn^{2+}$**
1003 **on $T_1$ relaxation in several brain regions.** ***A1,*** Mouse brain atlas-based segmentation of the
1004 primary (S1), secondary (S2) somatosensory cortex, globus pallidus, CA1, CA3, substantia nigra
1005 compacta (SNc), primary motor cortex (M1), secondary motor cortex (M2), and striatum. ROI,
1006 region of interest. ***A2***, Effects of $Mn^{2+}$ accumulation on increasing brain $T_1$ relaxation rate ($R_1$ in
1007 $msec^{-1}$). ***A3***, nifedipine treatment reduces the effects of $Mn^{2+}$ accumulation by reducing its
1008 concentration in brain. Thus, maps of mice treated with nifepidine had a slower rate of $T_1$
1009 relaxation, or lower $R_1$ in the case of the shown parametric maps (and lower intensity). Scale bar
1010 indicates intensity of $R_1$. ***B,*** A greater $Mn^{2+}$ accumulation produces faster rates of T1 relaxation
1011 ($R_1$) in VTA and SN than in other segmented cortical and subcortical nuclei ($F_{(9,72)} = 3.96$, $p <$
1012 0.001, one-way ANOVA followed by Tukey's test, $n = 8 – 9$ / group). **p < 0.01.
1013
1014 Supplemental movie 1: Representative live cell imaging of FFN200 release before and after $MnCl_2$.
1015 Supplemental movie 2: Representative live cell imaging of $Ca^{2+}$ mobilization before and after
1016 $MnCl_2$.
1017 Supplemental movie 3: Representative live cell imaging of $Ca^{2+}$ mobilization before and after
1018 NMDA (positive control groups).

1019

1020 Supplemental movie 4: Representative live cell TIRF imaging before and after $MnCl_2$.

1021

1022

1023

## References

Altschul SF, G. W., Miller, W., Myers, E. W. & Lipman, D. J. Basic local alignment search tool. *J. Mol. Biol.* **215,** 403-410 (1990).

Aoki, I., Naruse, S., & Tanaka, C. Manganese-enhanced magnetic resonance imaging (MEMRI) of brain activity and applications to early detection of brain ischemia. *NMR Biomed*. **17,** 569-580 (2004).

Aschner, J. L. & Aschner, M. Nutritional aspects of manganese homeostasis. *Mol Aspects Med.* **26**, 353-362 (2005).

Aschner, M., Guilarte, T.R., Schneider, J. S. & Zheng, W. Manganese: recent advances in understanding its transport and neurotoxicity. *Toxicol Appl Pharmacol* **221,** 131–47 (2007).

Aschner, M., Erikson, K. M., Herrero Hernández, E. & Tjalkens, R. Manganese and its role in Parkinson's disease: from transport to neuropathology. *Neuromolecular Med* **11,** 252-266 (2009).

Au, C., Benedetto, A. & Aschner, M. Manganese transport in eukaryotes: the role of DMT1. *Neurotoxicology* **29**, 569-576 (2008).

Bean, B. P. The action potential in mammalian central neurons. *Nat Rev Neurosci.* **8**, 451–465 (2007).

Benedetti, B., Matyash, V. & Kettenmann, H. Astrocytes control GABAergic inhibition of neurons in the mouse barrel cortex. *J Physiol* **589**(Pt 5), 1159-1172 (2011).

Bowman, A. B. & Aschner, M. Considerations on manganese (manganese) treatments for in vitro studies. *Neurotoxicology* **41**,141–142 (2014).

Bourinet, E. et al. The alpha 1E calcium channel exhibits permeation properties similar to low-voltage-activated calcium channels. *J Neurosci* **16**, 4983-4993 (1996).

Brenner, R. et al. Vasoregulation by the beta1 subunit of the calcium-activated potassium channel. *Nature* **407**, 870–876 (2000).

Cain, C. K., Blouin, A. M. & Barad, M. L-type voltage-gated calcium channels are required for extinction, but not for acquisition or expression, of conditional fear in mice. *J Neurosci* **22,** 9113-9121 (2002).

Chae, K. S. & Dryer, S. E. The p38 mitogen-activated protein kinase pathway negatively regulates $Ca^{2+}$-activated $K^{+}$ channel trafficking in developing parasympathetic neurons. *J Neurochem* **94**, 367–379 (2005).

Chen, C., Xu, Y., Zhang, J., Zhu, J., Zhang, J., Hu, N. & Guan, H. Altered expression of nNOS/NIDD in the retina of a glaucoma model of DBA/2J mice and the intervention by nNOS inhibition. *J Mol Neurosci* **51**, 47–56 (2013).

1057 Choi, D. W. Ionic dependence of glutamate neurotoxicity. *J Neurosci* **7**, 369-379 (1987).

1058 Choi, Y. M., Kim, S. H., Chung, S., Uhm, D. Y. & Park, M. K. Regional interaction of endoplasmic
1059 reticulum $Ca^{2+}$ signals between soma and dendrites through rapid luminal $Ca^{2+}$ diffusion. *J*
1060 *Neurosci* **26**, 12127-12136 (2006).

1061 Clapham, D. E. Calcium signaling. *Cell* **131**, 1047-1058 (2007).

1062 Crossgrove, J. & Zheng, W. Manganese toxicity upon overexposure. *NMR Biomed* **17**, 544–553
1063 (2004).

1064 Crossgrove, J. S. & Yokel, R. A. Manganese distribution across the blood–brain barrier: IV.
1065 Evidence for brain influx through store-operated calcium channels. *Neurotoxicology* **26**, 297–307
1066 (2005).

1067 Dodd, C. A., Ward, D. L. & Klein, B. G. Basal Ganglia accumulation and motor assessment
1068 following manganese chloride exposure in the C57BL/6 mouse. *Int J Toxicol* **24**, 389-397 (2005).

1069 Dodd, C. A., Bloomquist, J. R. & Klein, B. G. Consequences of manganese administration for
1070 striatal dopamine and motor behavior in 1-methyl-4-phenyl-1,2,3,6-tetrahydropyridine-exposed
1071 C57BL/6 mice. *Hum. Exp. Toxicol* **32**, 865–880 (2013).

1072 Cox, N., Toro, B., Pacheco-Otalora, L. F., Garrido-Sanabria, E. R. & Zarei, M. M. An endoplasmic
1073 reticulum trafficking signal regulates surface expression of β4 subunit of a voltage- and $Ca^{2+}$-
1074 activated K+ channel. *Brain Res* **1553**, 12–23 (2014).

1075 Erikson, K. M., Syversen, T., Aschner, J. L. & Aschner, M. Interactions between excessive
1076 manganese exposures and dietary iron-deficiency in neurodegeneration. *Environ Toxicol*
1077 *Pharmacol* **19**, 415–421 (2005).

1078 Fujishiro, H., Yoshida, M., Nakano, Y. & Himeno, S. Interleukin-6 enhances manganese
1079 accumulation in SH-SY5Y cells: implications of the up-regulation of ZIP14 and the down-
1080 regulation of ZnT10. *Metallomics*. **6**, 944-949 (2014).

1081 Gandhi, D., Sivanesan, S. & Kannan, K. Manganese-Induced Neurotoxicity and Alterations in
1082 Gene Expression in Human Neuroblastoma SH-SY5Y Cells. *Biol Trace Elem Res* **183**, 245-253
1083 (2018).

1084 Giordano, T. P. et al. Molecular switch from L-type Ca v 1.3 to Ca v 1.2 $Ca^{2+}$ channel signaling
1085 underlies long-term psychostimulant-induced behavioral and molecular plasticity. *J Neurosci* **30**,
1086 17051-62 (2010).

1087 Goodwin, J. S., Larson, G. A., Swant, J., Sen, N., Javitch, J. A., Zahniser, N. R., De Felice, L. J.
1088 & Khoshbouei, H. Amphetamine and methamphetamine differentially affect dopamine
1089 transporters in vitro and in vivo. *J Biol Chem* **284**, 2978–2989 (2009).

1090 Goytain, A., Hines, R. M. & Quamme, G. A. Huntingtin-interacting proteins, HIP14 and HIP14L,
1091 mediate dual functions, palmitoyl acyltransferase and $Mg^{2+}$ transport. *J. Biol. Chem* **283**, 33365–
1092 33374 (2008).

1093 Greene, A. C & Madgwick, J. C. Heterotrophic manganese-oxidizing bacteria from Groote
1094 Eylandt, Australia. *Geomicrobiol J* **6**, 119–127 (1988).

1095 Guilarte, T. R. Manganese and Parkinson's disease: A critical review and new findings. *Environ.*
1096 *Health Perspect* **118**, 1071–1080 (2010).

1097 Gunshin, H. et al. Cloning and characterization of a mammalian proton-coupled metal-ion
1098 transporter. *Nature* **388**, 482–488 (1997).

1099 Gunter, T. E., Gerstner, B., Gunter, K. K., Malecki, J., Gelein, R., Valentine, W. M., Aschner, M.
1100 & Yule, D. I. Manganese transport via the transferrin mechanism. *Neurotoxicology* **34**, 118–127
1101 (2013).

1102 Guzman, J. N., Sánchez-Padilla, J., Chan, C. S. & Surmeier, D. J. Robust pacemaking in substantia
1103 nigra dopaminergic neurons. *J Neurosci* **29**, 11011–11019 (2009).

1104 Higashi, Y., Asanuma, M., Miyazaki, I., Hattori, N., Mizuno, Y. & Ogawa, N. Parkin attenuates
1105 manganese-induced dopaminergic cell death. *J Neurochem* **89**, 1490-1497 (2004).

1106 Itoh, K., Sakata, M., Watanabe, M., Aikawa, Y. & Fujii, H. The entry of manganese ions into the
1107 brain is accelerated by the activation of N-methyl-D-aspartate receptors. *Neuroscienc*e **154**, 732–
1108 740 (2008).

1109 Jankovic, J. Searching for a relationship between manganese and welding and Parkinson's disease.
1110 *Neurology* **64**, 2021-2018 (2005).

1111 Jenkinson, M., Bannister, P., Brady, M. & Smith, S. Improved optimization for the robust and
1112 accurate linear registration and motion correction of brain images. *Neuroimage*. **17**, 825-841
1113 (2002).

1114 Jinnah, H. A., Yitta, S., Drew, T., Kim, B. S., Visser, J. E. & Rothstein JD Calcium channel
1115 activation and self-biting in mice. *Proc Natl Acad Sci U S A* **96**, 15228-15232 (1999).

1116 Josephs, K. A., Ahlskog, J. E., Klos, K. J., Kumar, N., Fealey, R. D., Trenerry, M. R. & Cowl, C.
1117 T. Neurologic manifestations in welders with pallidal MRI T1 hyperintensity. *Neurology* **64**, 2033-
1118 2039 (2005).

1119 Kessler, K. R., Wunderlich, G., Hefter, H. & Seitz, R. J. Secondary progressive chronic
1120 manganism associated with markedly decreased striatal D2 receptor density. *Mov Disord* **18**, 217-
1121 218 (2003).

1122 Kitazawa, M., Anantharam, V., Yang, Y., Hirata, Y., Kanthasamy, A. & Kanthasamy, A. G.
1123 Activation of protein kinase C delta by proteolytic cleavage contributes to manganese-induced
1124 apoptosis in dopaminergic cells: protective role of Bcl-2. *Biochem. Pharmacol* **69**, 133–146 (2005).

1125 Knaus, H. G., Garcia-Calvo, M., Kaczorowski, G. J. & Garcia, M. L. Subunit composition of the
1126 high conductance calcium-activated potassium channel from smooth muscle, a representative of
1127 the mSlo and slowpoke family of potassium channels. *J Biol Chem* **269**, 3921–3924 (1994).

1128 Lauterbur, P. C. Progress in n.m.r. zeugmatography imaging. *Philos Trans R Soc Lond B Biol Sci.*
1129 **289**(1037), 483-487 (1980).

1130 Lee, J. H., Silva, A. C., Merkle, H & Koretsky, A. P. Manganese-enhanced magnetic resonance
1131 imaging of mouse brain after systemic administration of $MnCl_2$: dose-dependent and temporal
1132 evolution of T1 contrast. *Magn Reson Med* **53**, 640-648 (2005).

1133 Leyva-Illades, D. et al. SLC30A10 is a cell surface-localized manganese efflux transporter, and
1134 Parkinsonism-causing mutations block its intracellular trafficking and efflux activity. *J. Neurosci*
1135 **34**, 14079–14095 (2014).

1136 Lin, M., Sambo, D. & Khoshbouei, H. Methamphetamine Regulation of Firing Activity of
1137 Dopamine Neurons. *J Neurosci* **36**, 10376-10391 (2016).

1138 Liu, X., Sullivan, K. A., Madl, J. E., Legare, M. & Tjalkens, R. B. Manganese-induced
1139 neurotoxicity: the role of astroglial-derived nitric oxide in striatal interneuron degeneration.
1140 *Toxicol Sci* **91**, 521-31 (2006).

1141 Lockman, P. R., Roder, K. E. & Allen, D. D. Inhibition of the rat blood-brain barrier choline
1142 transporter by manganese chloride. *J. Neurochem* **79**, 588–594 (2001).

1143 Lu, R., Alioua, A., Kumar, Y., Eghbali, M., Stefani, E & Toro, L. MaxiK channel partners:
1144 physiological impact. *J Physiol* **570**, 65–72 (2006).

1145 Madison, J. L., Wegrzynowicz, M., Aschner, M. & Bowman, A. B. Disease-toxicant interactions
1146 in manganese exposed huntington disease mice: Early changes in striatal neuron morphology and
1147 dopamine metabolism. *PLoS One* 7: e31024 (2012).

1148 Martinez-Finley, E. J., Gavin, C. E., Aschner, M. & Gunter, T. E. Manganese neurotoxicity and
1149 the role of reactive oxygen species. *Free Radic Biol Med*. **62**, 65-75 (2013).

1150 Mercuri, N. B., Bonci, A., Calabresi, P., Stratta, F., Stefani, A. & Bernardi, G. Effects of
1151 dihydropyridine calcium antagonists on rat midbrain dopaminergic neurones. *Br. J. Pharmacol*
1152 **113**, 831–838 (1994).

1153 Michalke, B. & Fernsebner, K. New insights into manganese toxicity and speciation. *J Trace Elem*
1154 *Med Biol* **28**, 106-116 (2014).

1155 Morellini F. et al. Impaired Fear Extinction Due to a Deficit in $Ca^{2+}$ Influx Through L-Type
1156 Voltage-Gated $Ca^{2+}$ Channels in Mice Deficient for Tenascin-C. *Front Integr Neurosci* doi:
1157 10.3389/fnint (2017).

1158 Morikawa, H. & Paladini, C. A. Dynamic regulation of midbrain dopamine neuron activity:
1159 intrinsic, synaptic, and plasticity mechanisms. *Neuroscience*. **198**, 95-111 (2011).

1160 Nedergaard, S., Flatman, J. A. & Engberg, I. Nifedipine- and omega-conotoxin-sensitive $Ca^{2+}$
1161 conductances in guinea-pig substantia nigra pars compacta neurones. *J. Physiol* **466**, 727–747
1162 (1993).

1163 Olanow, C. W. Manganese-induced parkinsonism and Parkinson's disease. *Ann N Y Acad Sci.* **1012**,
1164 209-223 (2004).

1165 Perl, D. P. & Olanow, C. W. The neuropathology of manganese-induced parkinsonism. *J.*
1166 *Neuropathol. Exp. Neurol* **66**, 675–682 (2007).

1167 Pereira, D.B. et al. Fluorescent false neurotransmitter reveals functionally silent dopamine vesicle
1168 clusters in the striatum. *Nat Neurosci*. 19:578-586 (2016).

1169 Persson, I. Hydrated metal ions in aqueous solution: How regular are their structures? *Pure Appl.*
1170 *Chem* **82**, 901–1917 (2010).

1171 Poole, D. S., Doorenweerd, N., Plomp. J. J., Mahfouz, A., Reinders, M. J. T. & van der Weerd, L.
1172 Continuous infusion of manganese improves contrast and reduces side effects in manganese-
1173 enhanced magnetic resonance imaging studies. *Neuroimage* **147**, 1-9 (2017).

1174 Puopolo, M., Raviola, E. & Bean, B. P. Roles of subthreshold calcium current and sodium current
1175 in spontaneous firing of mouse midbrain dopamine neurons. *J Neurosci* **27**, 645-656 (2007).

1176 Puskin, J. S. & Gunter, T. E. Ion and pH gradients across the transport membrane of mitochondria
1177 following $Mn^{++}$ uptake in the presence of acetate. *Biochem Biophys Res Commun* **51**, 797-803
1178 (1973).

1179 Putzier, I., Kullmann, P. H., Horn, J. P. & Levitan, E. S. Cav1.3 channel voltage dependence, not
1180 $Ca^{2+}$ selectivity, drives pacemaker activity and amplifies bursts in nigral DA neurons. *J Neurosci*
1181 **29**, 15414–15419 (2009).

1182 Rogers, K., Beaubrun, I., Catapane, E. & Carroll, M. The toxic effects of manganese on dopamine
1183 D2 receptor activation is not due to inactivation of the phospholipase c receptor signal transduction
1184 component (1143.7). *FASEB J* **28**:1143.7 (2014).

1185 Roth, J. A., Li, Z., Sridhar, S. & Khoshbouei, H. The effect of manganese on dopamine toxicity
1186 and dopamine transporter (DAT) in control and DAT transfected HEK cells. *Neurotoxicology* **35**,
1187 121–128 (2013).

1188 Saha, K., Sambo, D., Richardson, B. D., Lin, L. M., Butler, B., Villarroel, L. & Khoshbouei, H.
1189 Intracellular methamphetamine prevents the dopamine-induced enhancement of neuronal firing. *J*
1190 *Biol Chem* **289**, 22246-57 (2014).

1191 Sambo, D. O. et al. The sigma-1 receptor modulates methamphetamine dysregulation of dopamine
1192 neurotransmission. *Nat Commun*. **20**;8(1):2228. doi: 10.1038/s41467-017-02087-x (2017).

1193 Schmidt, K. F. et al. Volume reconstruction techniques improve the correlation between
1194 histological and in vivo tumor volume measurements in mouse models of human gliomas. *J*
1195 *Neurooncol* **68**, 207-215 (2004).

1196 Seth, P. K. & Chandra, S. V. Neurotransmitters and neurotransmitter receptors in developing and
1197 adult rats during manganese poisoning. *Neurotoxicology* **5**, 67–76 (1984).

1198 Shruti, S., Urban-Ciecko, J., Fitzpatrick, J. A., Brenner, R., Bruchez, M. P. & Barth, A. L. The
1199 brain-specific beta4 subunit downregulates BK channel cell surface expression. *PLoS One* **7**,
1200 e33429 (2012).

1201 Soriano, S. et al. Metal Homeostasis Regulators Suppress FRDA Phenotypes in a Drosophila
1202 Model of the Disease. *PLoS One* **11**:e0159209 (2016).

1203 Streifel, K. M., Miller, J., Mouneimne, R. & Tjalkens, R. B. Manganese inhibits ATP-induced
1204 calcium entry through the transient receptor potential channel TRPC3 in astrocytes.
1205 *Neurotoxicology* **34**, 160-166 (2013).

1206 Tjalkens, R. B., Zoran, M. J., Mohl, B. & Barhoumi, R. Manganese suppresses ATP-dependent
1207 intercellular calcium waves in astrocyte networks through alteration of mitochondrial and
1208 endoplasmic reticulum calcium dynamics. *Brain Res* **1113**, 210-219 (2006).

1209 Torkkeli, P. H., Meisner, S., Pfeiffer, K. & French, A. S. GABA and glutamate receptors have
1210 different effects on excitability and are differentially regulated by calcium in spider
1211 mechanosensory neurons. *Eur J Neurosci* **36**, 3602-3614 (2012).

1212 Toro, B., Cox, N., Wilson, R. J., Garrido-Sanabria, E., Stefani, E., Toro, L & Zarei, M. M.
1213 KCNMB1 regulates surface expression of a voltage and $Ca^{2+}$-activated $K^{+}$ channel via endocytic
1214 trafficking signals. *Neuroscience* **142**, 661–669 (2006).

1215 Tuschl, K., Mills, P. B. & Clayton, P. T. Manganese and the brain. *Int Rev Neurobiol* **110**, 277–
1216 312 (2013).

1217 Uchino, A., Noguchi, T., Nomiyama, K., Takase, Y., Nakazono, T., Nojiri, J. & Kudo, S.
1218 Manganese accumulation in the brain: MR imaging. *Neuroradiology* **49**, 715–720 (2007).

1219 Verhoeven, W. M., Egger, J. I. & Kuijpers, H. J. Manganese and acute paranoid psychosis: a case
1220 report. *J Med Case Rep* **5**:146. doi: 10.1186/1752-1947-5-146 (2011).

1221 Wang, B., Rothberg, B. S. & Brenner, R. Mechanism of increased BK channel activation from a
1222 channel mutation that causes epilepsy. *J Gen Physiol* **133**, 283–294 (2009).

1223 Waterhouse, A. et al. SWISS-MODEL: homology modelling of protein structures and complexes.
1224 *Nucleic Acids Res* **46**(W1), W296-W303 (2018).

1225 Weiger, T. M., Hermann, A. & Levitan, I. B. Modulation of calcium-activated potassium channels.
1226 *J. Comp. Physiol. A Neuroethol. Sens. Neural. Behav. Physiol* **188**, 79–87 (2002).

White, R. E., Schonbrunn, A. & Armstrong, D. L. Somatostatin stimulates $Ca^{2+}$-activated $K^{+}$ channels through protein dephosphorylation. *Nature* **351**:570–573 (1991).

Wild, A. R., Jones, S. & Gibb, A. J. Activity-dependent regulation of NMDA receptors in substantia nigra dopaminergic neurones. *J Physiol* **592**, 653-668 (2014).

Wu, J. P., Yan, Z., Li, Z. Q., Qian, X. Y., Lu, S., Dong, M. Q., Zhou Q. & Yan, N. Structure of the voltage-gated calcium channel Ca(v)1.1 at 3.6 Å resolution. *Nature* **537**, 191-196 (2016).

Xu, B., Xu, ZF. & Deng, Y. Effect of manganese exposure on intracellular $Ca^{2+}$ homeostasis and expression of NMDA receptor subunits in primary cultured neurons. *Neurotoxicology* **30**, 941-949 (2009).

Zhang, D. Q., Stone, J. F., Zhou, T., Ohta, H. & McMahon, D. G. Characterization of genetically labeled catecholamine neurons in the mouse retina. *Neuroreport* **15**, 1761–1765 (2004).

Zogzas, C. E. & Mukhopadhyay, S. Inherited Disorders of Manganese Metabolism. *Adv Neurobiol* **18**, 35-49 (2017).

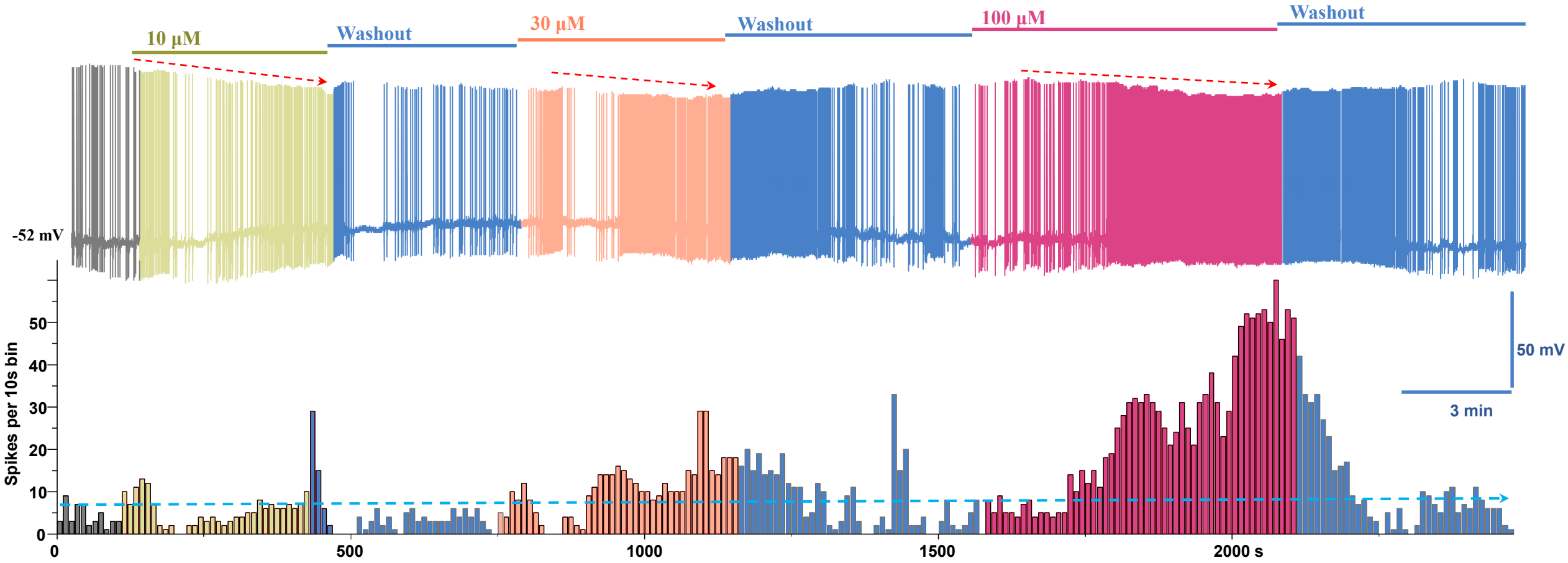
10 µM
Washout
30 µM
Washout
100 µM
Washout
-52 mV
Spikes per 10s bin
0
10
20
30
40
50
0
500
1000
1500
2000 s
50 mV
3 min

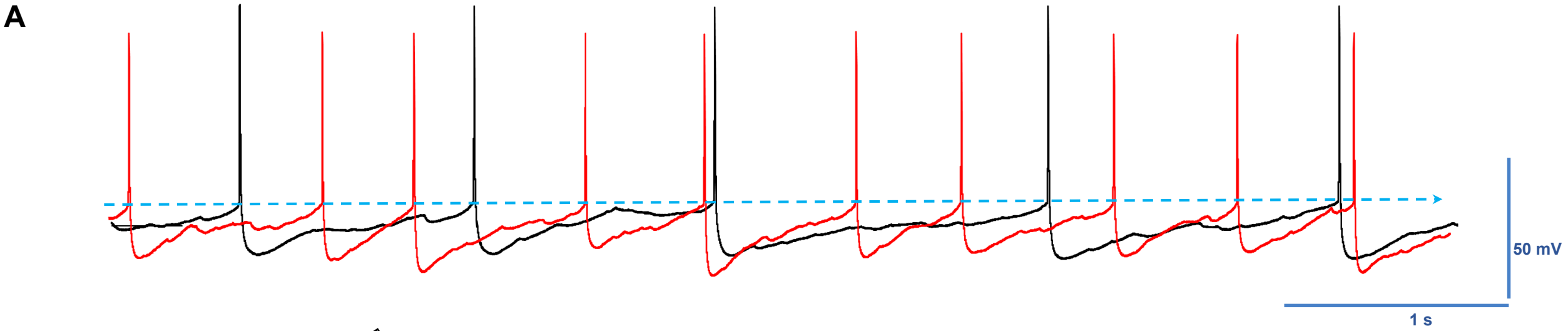


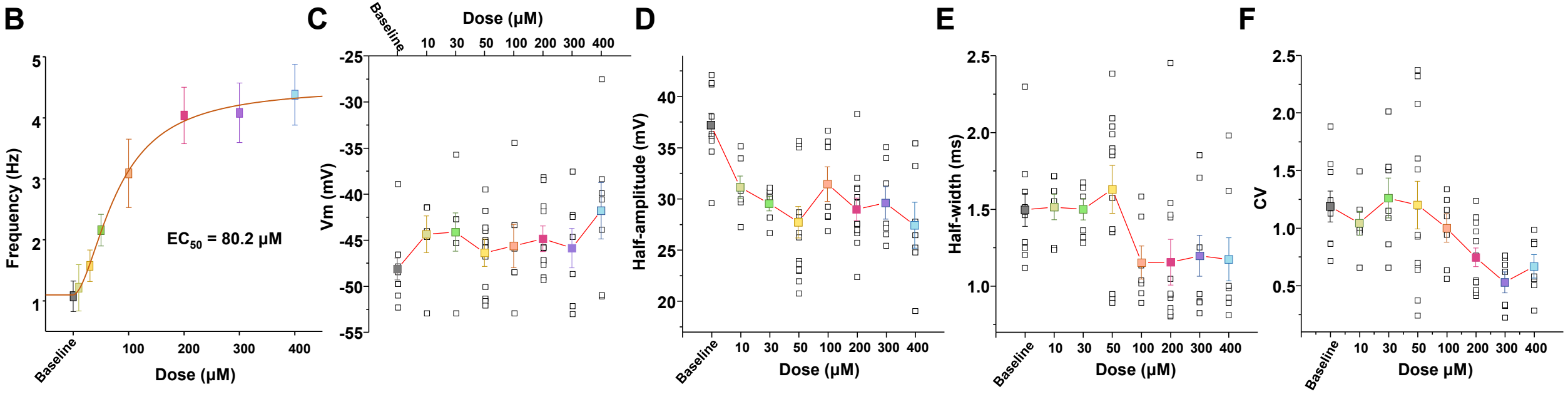


Baseline: 1.08 ± 0.2 Hz (n = 10)
10: 1.21± 0.4 Hz (n = 6, p = 0.73)
30: 1.57 ± 0.3 Hz (n = 7, p = 0.14)
50: 2.16 ± 0.3 Hz (n = 7, p = 0.3)
100: 3.09 ± 0.6 Hz (n = 7, p = 0.0006)
200: 4.04 ± 0.5 Hz (n = 13, p < 0.00001)
300: 4.08± 0.5 Hz (n = 7, p < 0.00001)
400: 4.38± 0.5 Hz (n = 6, p < 0.00001)

Baseline: -48.1 ± 1.2 mV (n = 10)
10: -44.3 ± 2.0 mV (n = 6, p = 0.09)
30: -44.1 ± 2.1 mV (n = 7, p = 0.08 )
50: -46.3 ± 1.5 mV (n = 13, p = 0.29 )
100: -45.6 ± 2.4 mV (n = 7, p = 0.29)
200: -44.8 ± 1.4 mV (n = 13, p = 0.048)
300: -45.8 ± 2.1 mV (n = 7, p = 0.33)
400: -41.8 ± 3.1 mV (n = 7, p = 0.045)

Baseline: 37.2 ± 1.1 mV (n = 11)
10: 31.1 ± 1.1 mV (n = 6, p = 0.003)
30: 29.5 ± 0.7 mV (n = 6, p = 0.0002)
50: 27.7 ± 1.5 mV (n = 14, p = 0.00005)
100: 31.4 ± 1.7 mV (n = 7, p = 0.006)
200: 29.0 ± 1.1 mV (n = 13, p = 0.00002)
300: 29.6 ± 1.6 mV (n = 7, p = 0.0006)
400: 27.4 ± 2.2 mV (n = 7, p = 0.0003)

Baseline: 1.5 ± 0.1 ms (n = 10)
10: 1.5 ± 0.02 ms (n = 6, p = 0.91)
30: 1.5 ± 0.07 ms (n = 7, p = 0.98)
50: 1.6 ± 0.15 ms (n = 13, p = 0.47)
100: 1.15 ± 0.1 ms (n = 7, p = 0.04)
200: 1.15 ± 0.1 ms (n = 13, p = 0.02)
300: 1.19 ± 0.1 ms (n = 7, p = 0.12)
400: 1.17 ± 0.1 ms (n = 7, p = 0.11)

Baseline: 1.18 ± 0.1 (n = 11)
10: 1.04 ± 0.1 (n = 6, p = 0.40)
30: 1.26 ± 0.2 (n = 7, p = 0.71)
50: 1.20 ± 0.2 (n = 13, p = 0.96)
100: 1.00 ± 0.1 (n = 7, p = 0.26)
200: 0.74 ± 0.08 (n = 13, p = 0.0025)
300: 0.53 ± 0.09 (n = 7, p = 0.0005)
400: 0.66 ± 0.1 (n = 7, p = 0.004)

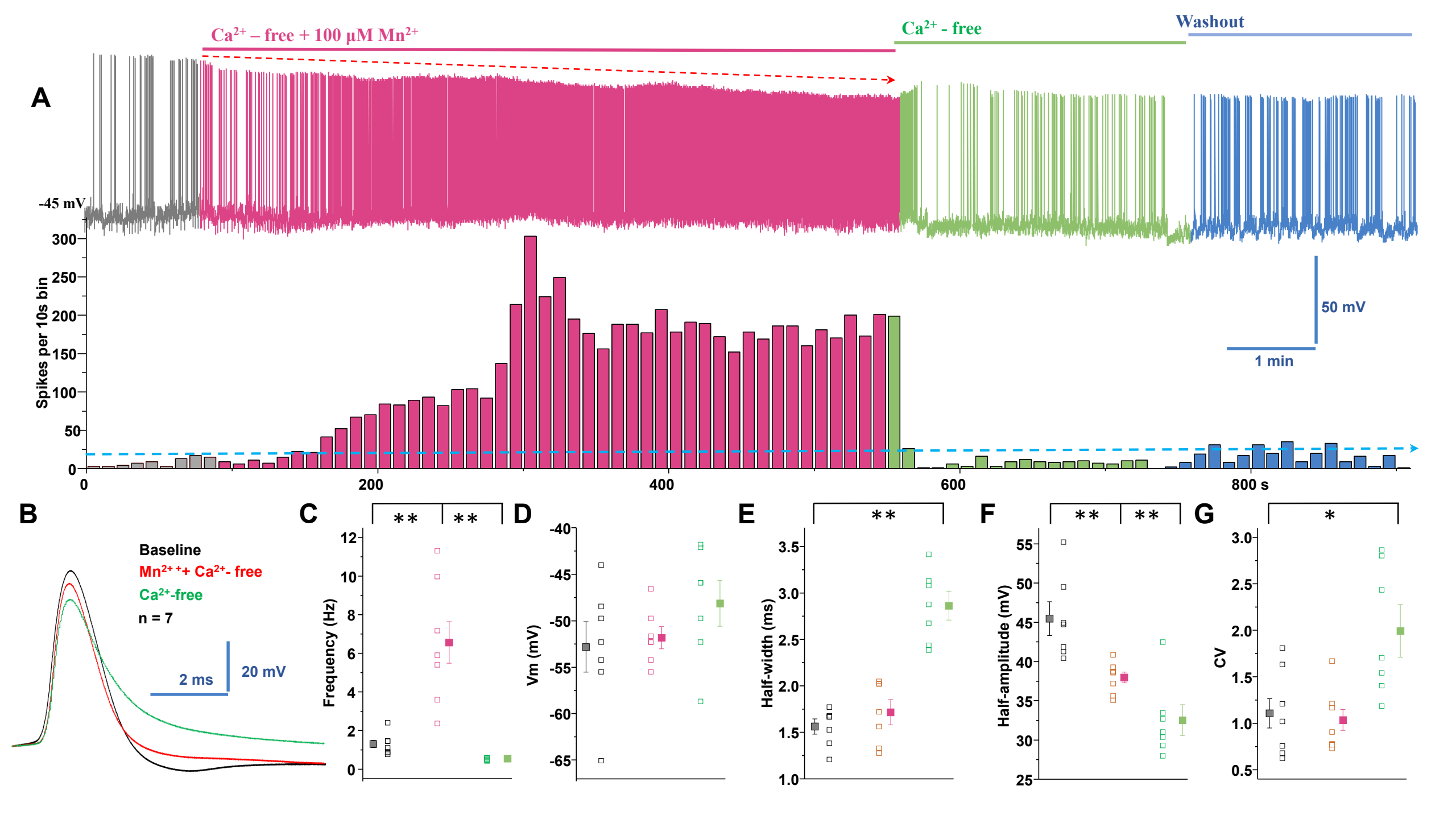
A
Ca2+ – free + 100 µM Mn2+
Ca2+ - free
Washout
-45 mV
50 mV
1 min
Spikes per 10s bin
0
50
100
150
200
250
300
0
200
400
600
800 s
B
Baseline
Mn2+ +Ca2+- free
Ca2+-free
n = 7
2 ms
20 mV
C
Frequency (Hz)
**
**
D
Vm (mV)
E
Half-width (ms)
**
F
Half-amplitude (mV)
**
**
G
CV
*

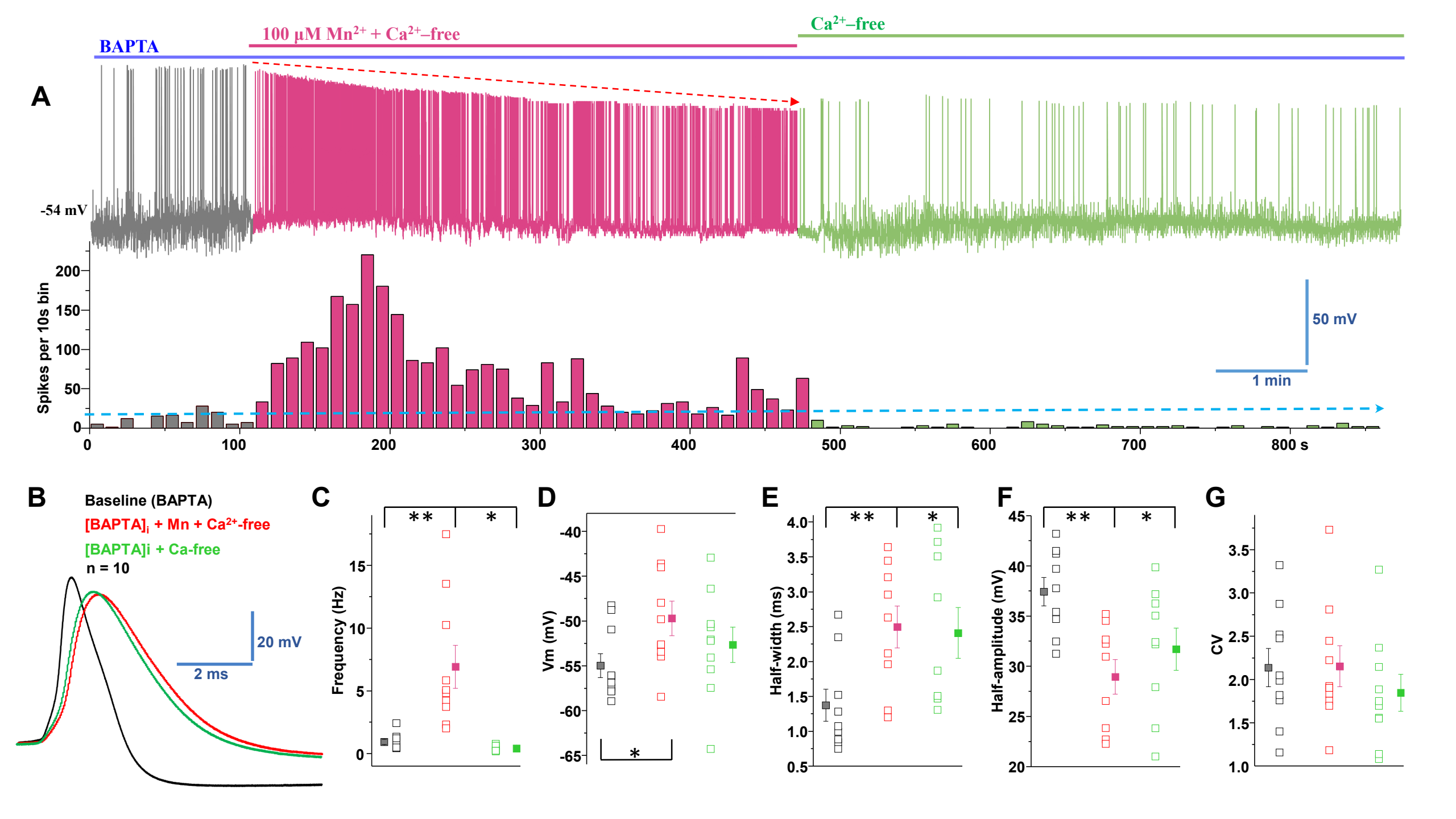
BAPTA
100 µM Mn2+ + Ca2+–free
Ca2+–free
A
-54 mV
Spikes per 10s bin
50 mV
1 min
0
100
200
300
400
500
600
700
800 s
B
Baseline (BAPTA)
[BAPTA]i + Mn + Ca2+-free
[BAPTA]i + Ca-free
n = 10
20 mV
2 ms
C
Frequency (Hz)
D
Vm (mV)
E
Half-width (ms)
F
Half-amplitude (mV)
G
CV

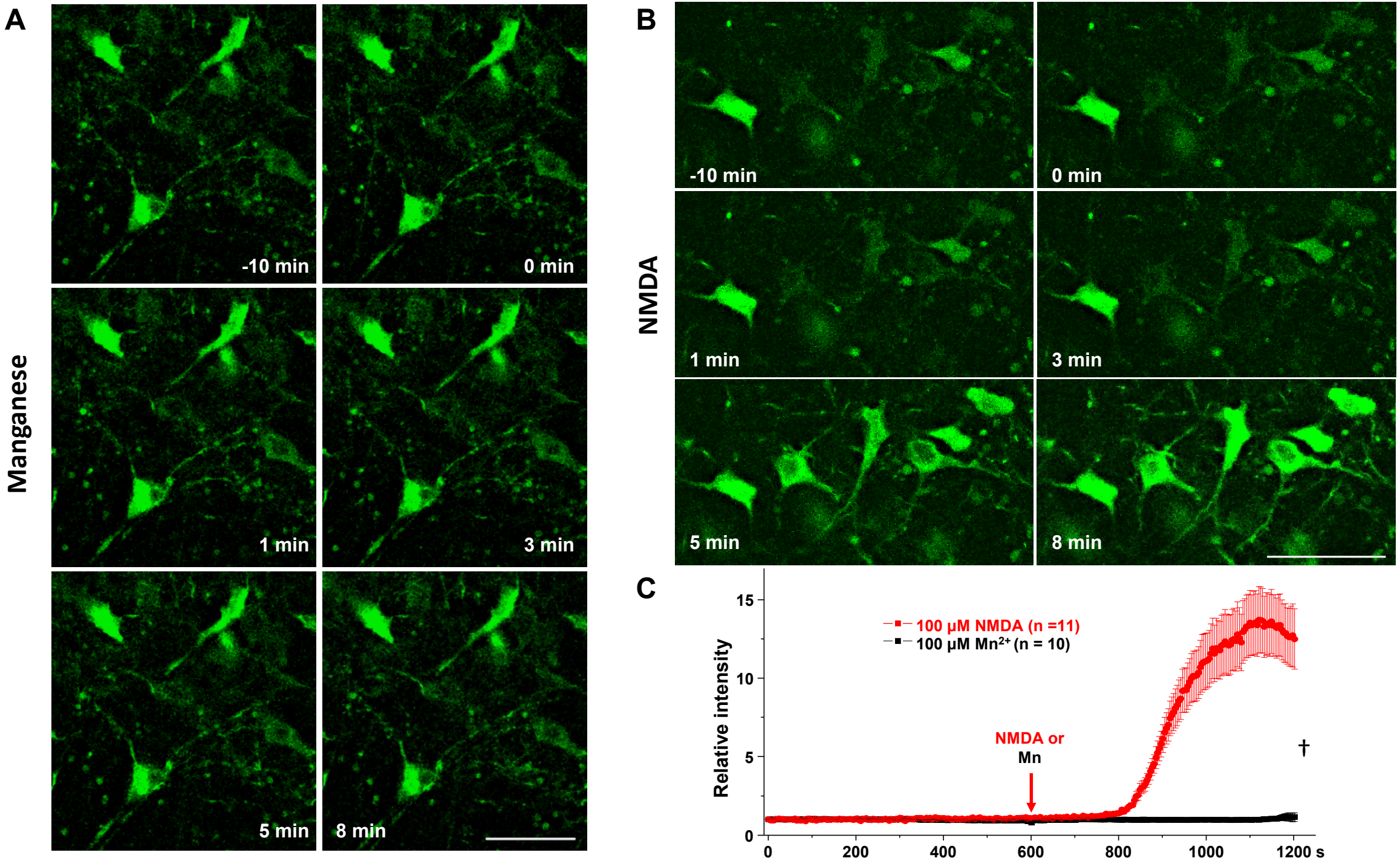
A
Manganese
-10 min
0 min
1 min
3 min
5 min
8 min
B
NMDA
-10 min
0 min
1 min
3 min
5 min
8 min
C
Relative intensity
100 μM NMDA (n =11)
100 μM Mn2+ (n = 10)
NMDA or
Mn
†
0
5
10
15
0
200
400
600
800
1000
1200 s

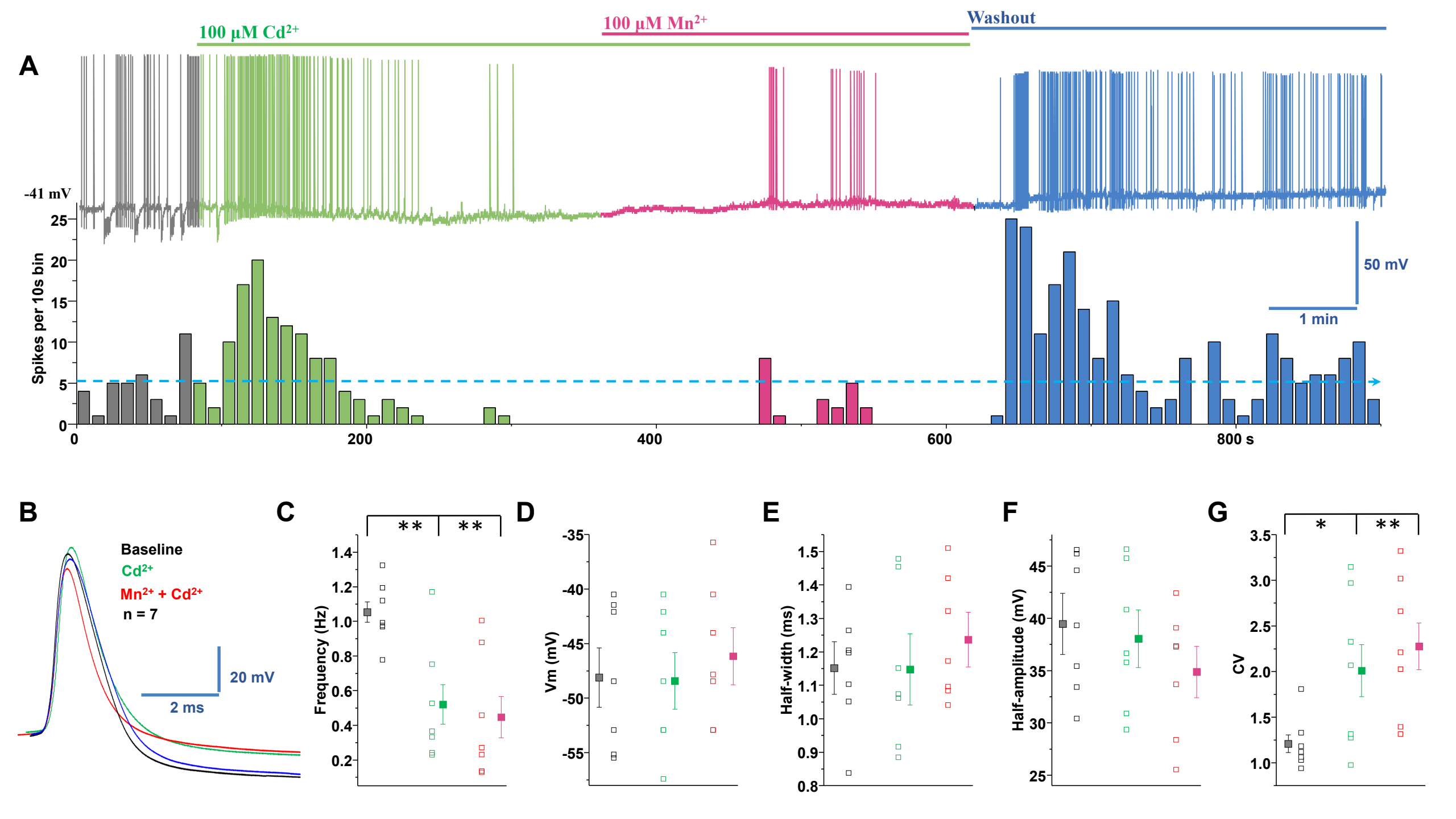
100 µM Cd2+
100 µM Mn2+
Washout
A
-41 mV
Spikes per 10s bin
50 mV
1 min
0
200
400
600
800 s
B
Baseline
Cd2+
Mn2+ + Cd2+
n = 7
20 mV
2 ms
C
Frequency (Hz)
**
**
D
Vm (mV)
E
Half-width (ms)
F
Half-amplitude (mV)
G
CV
*
**

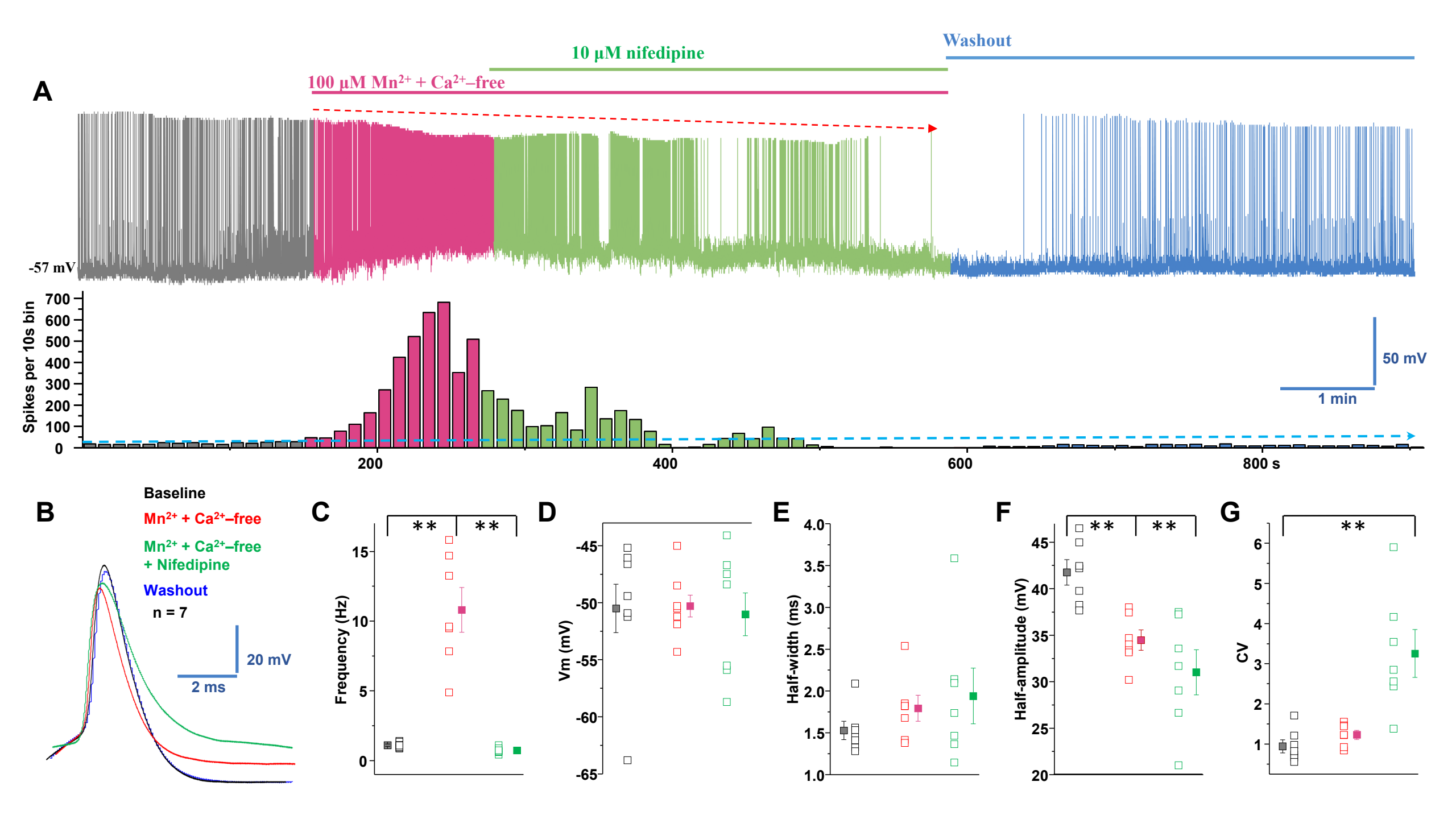
A
Washout
10 µM nifedipine
100 µM Mn2+ + Ca2+–free
-57 mV
Spikes per 10s bin
700
600
500
400
300
200
100
0
200
400
600
800 s
50 mV
1 min
B
Baseline
Mn2+ + Ca2+–free
Mn2+ + Ca2+–free
+ Nifedipine
Washout
n = 7
20 mV
2 ms
C
Frequency (Hz)
15
10
5
0
**
**
D
Vm (mV)
-45
-50
-55
-60
-65
E
Half-width (ms)
4.0
3.5
3.0
2.5
2.0
1.5
1.0
F
Half-amplitude (mV)
45
40
35
30
25
20
**
**
G
CV
6
5
4
3
2
1
**

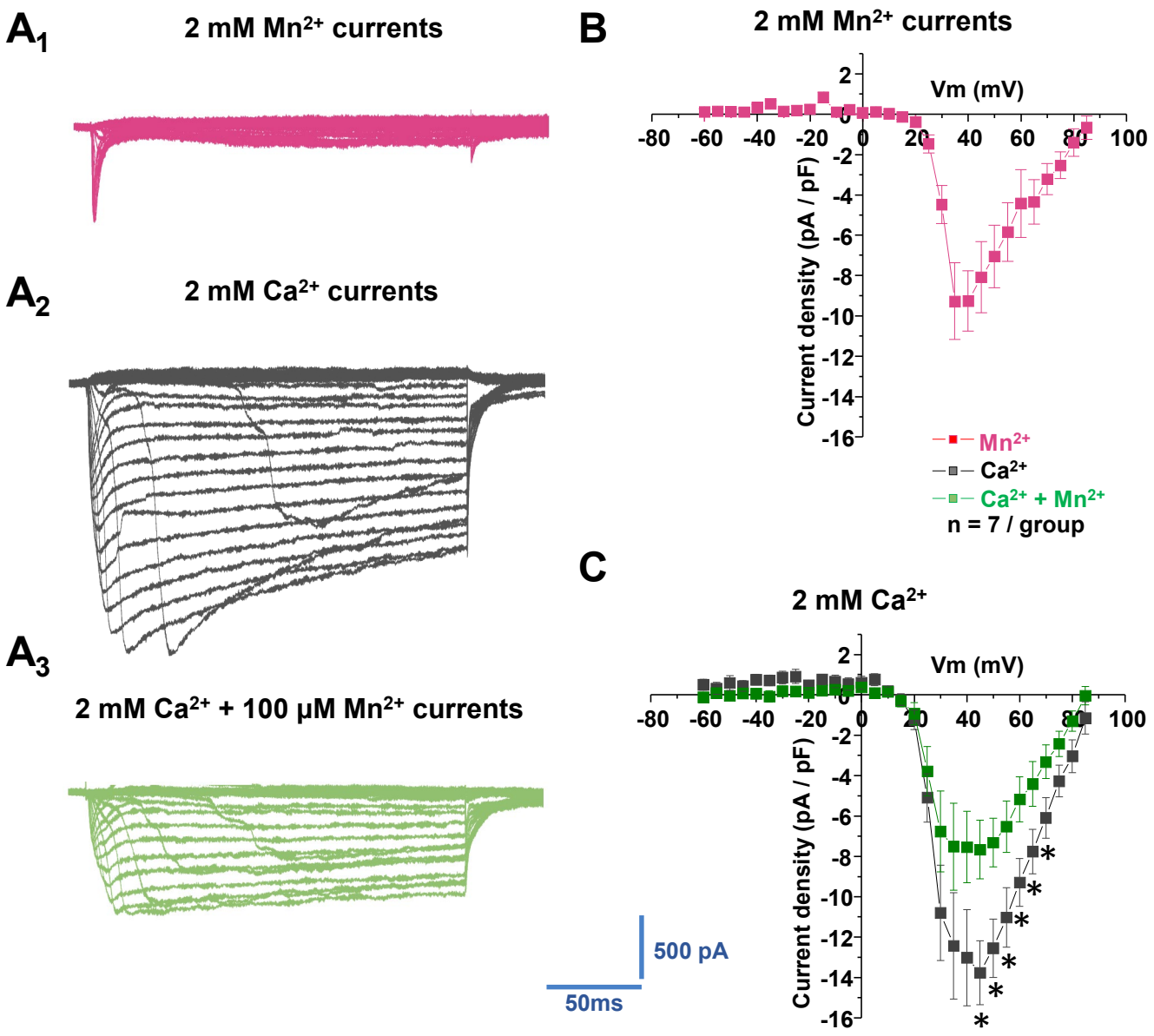
A1
2 mM Mn2+ currents
A2
2 mM Ca2+ currents
A3
2 mM Ca2+ + 100 μM Mn2+ currents
500 pA
50ms
B
2 mM Mn2+ currents
Vm (mV)
Current density (pA / pF)
Mn2+
Ca2+
Ca2+ + Mn2+
n = 7 / group
C
2 mM Ca2+
Vm (mV)
Current density (pA / pF)

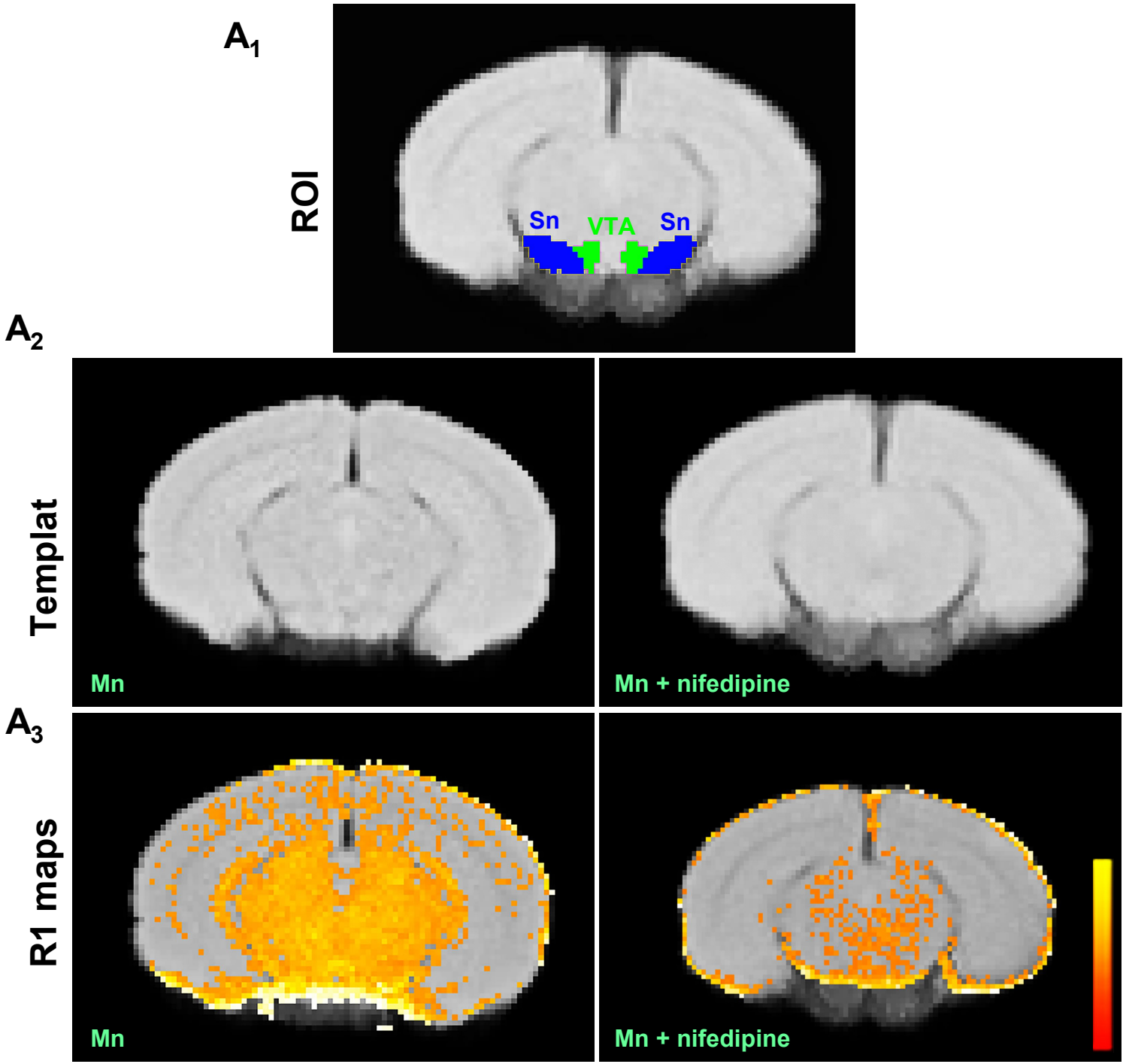
A1
ROI
Sn
VTA
Sn
A2
Templat
Mn
Mn + nifedipine
A3
R1 maps
Mn
Mn + nifedipine

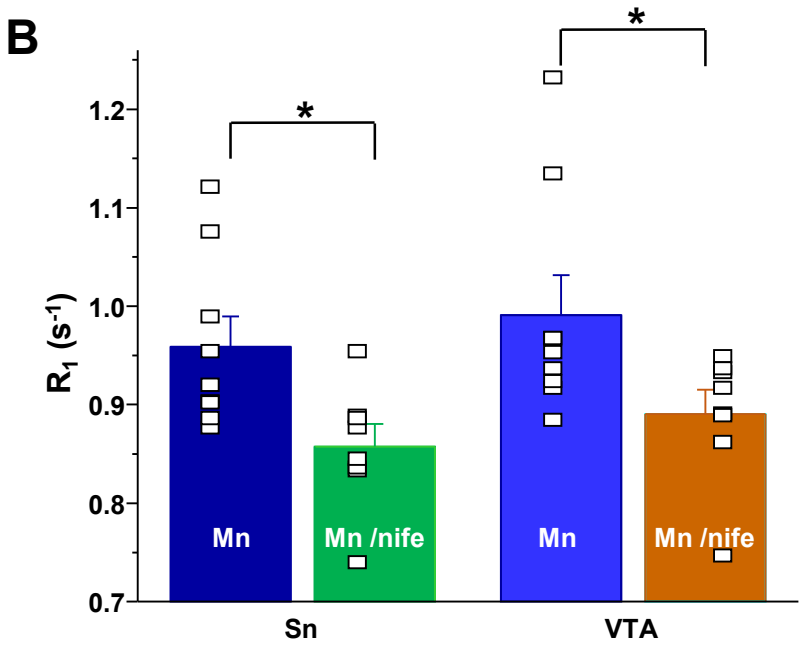
B
R1 (s-1)
1.2
1.1
1.0
0.9
0.8
0.7
*
*
Mn
Mn /nife
Mn
Mn /nife
Sn
VTA

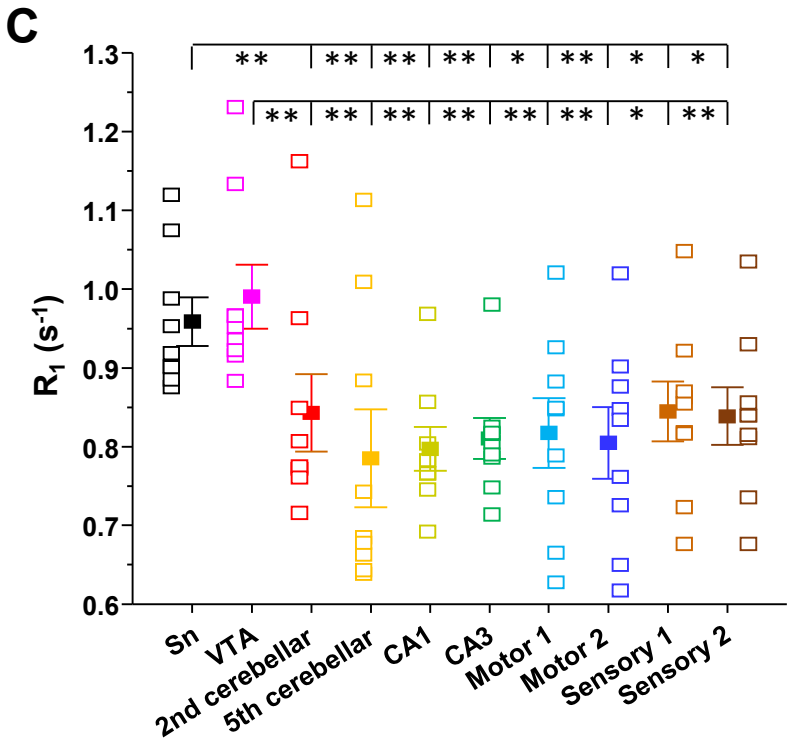
C
R1 (s-1)
1.3
1.2
1.1
1.0
0.9
0.8
0.7
0.6
Sn
VTA
2nd cerebellar
5th cerebellar
CA1
CA3
Motor 1
Motor 2
Sensory 1
Sensory 2

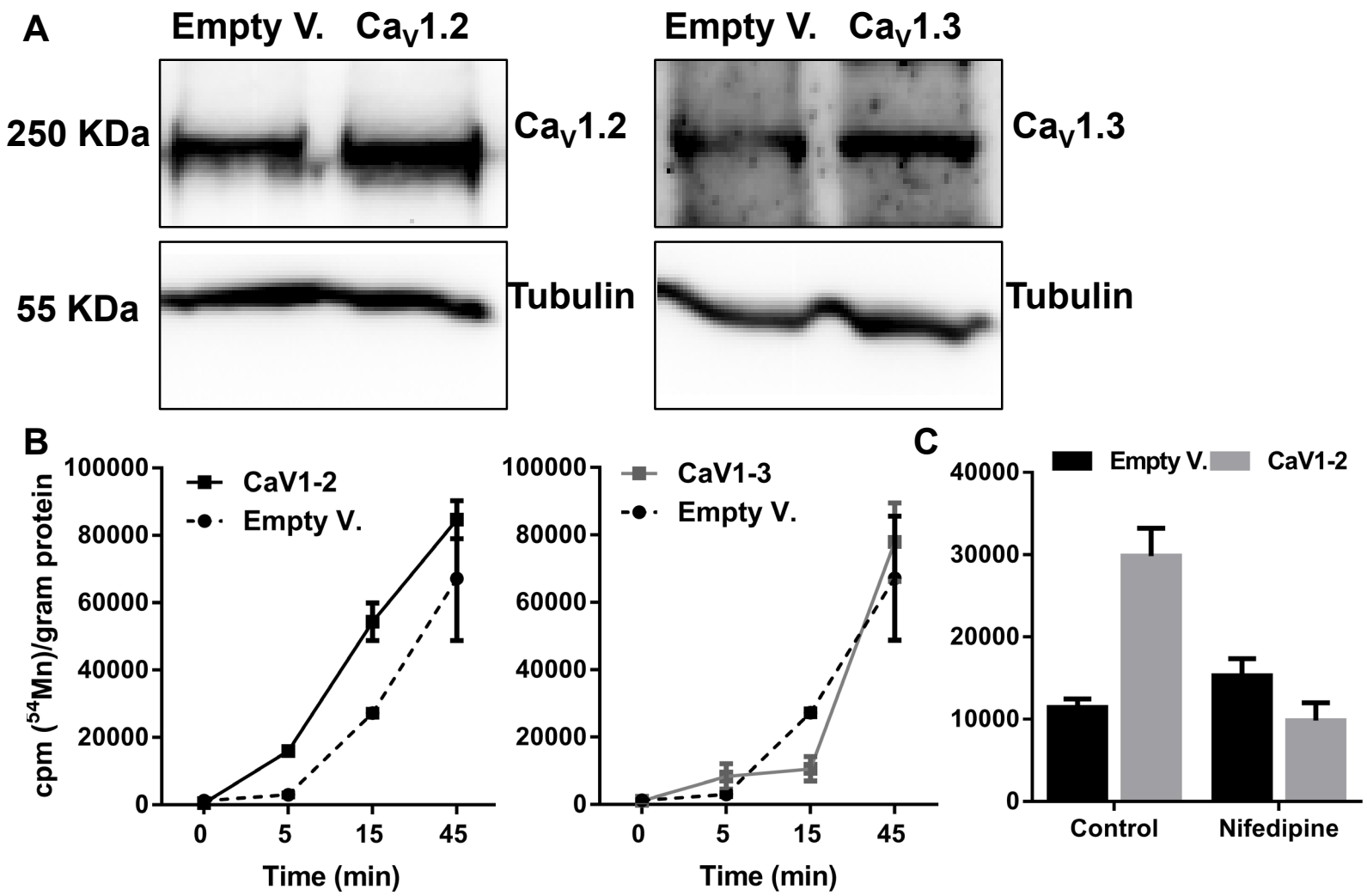
A
Empty V.
$Ca_V1.2$
Empty V.
$Ca_V1.3$
250 KDa
$Ca_V1.2$
$Ca_V1.3$
55 KDa
Tubulin
Tubulin
B
cpm ($^{54}$Mn)/gram protein
100000
80000
60000
40000
20000
0
CaV1-2
Empty V.
0
5
15
45
Time (min)
CaV1-3
Empty V.
Time (min)
C
Empty V.
CaV1-2
40000
30000
20000
10000
0
Control
Nifedipine

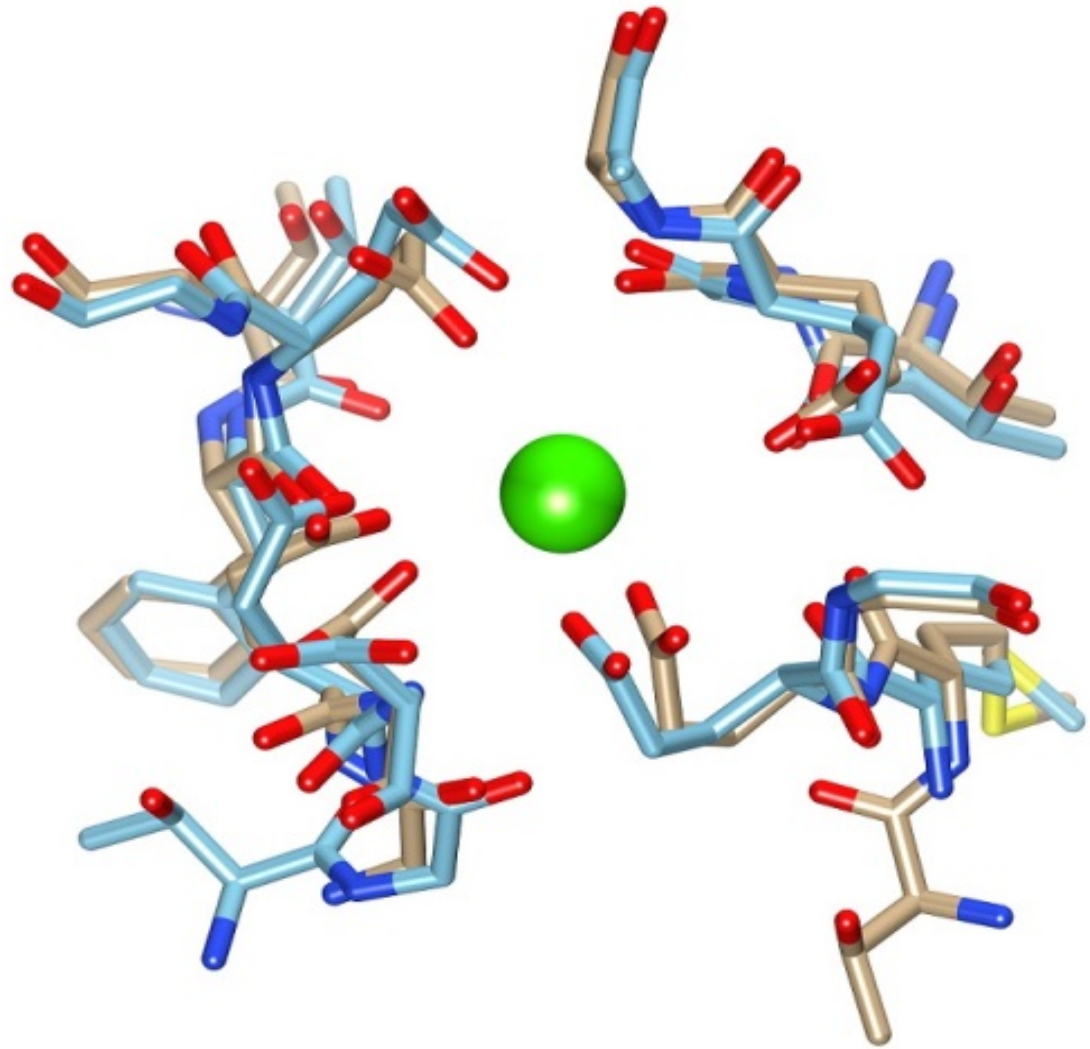

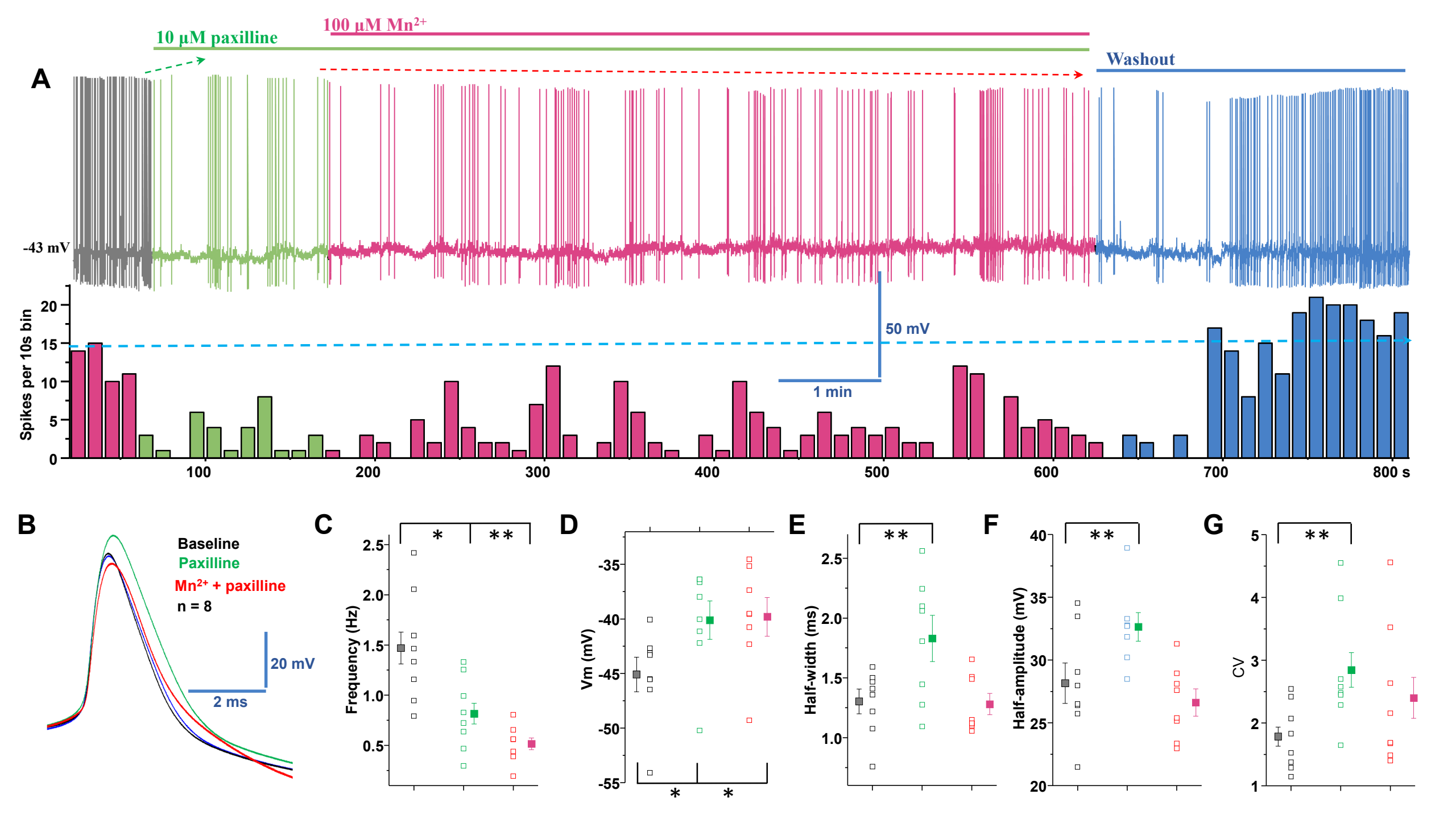
A
10 µM paxilline
100 µM Mn2+
Washout
-43 mV
Spikes per 10s bin
50 mV
1 min
100
200
300
400
500
600
700
800 s
B
Baseline
Paxilline
Mn2+ + paxilline
n = 8
20 mV
2 ms
C
Frequency (Hz)
D
Vm (mV)
E
Half-width (ms)
F
Half-amplitude (mV)
G
CV

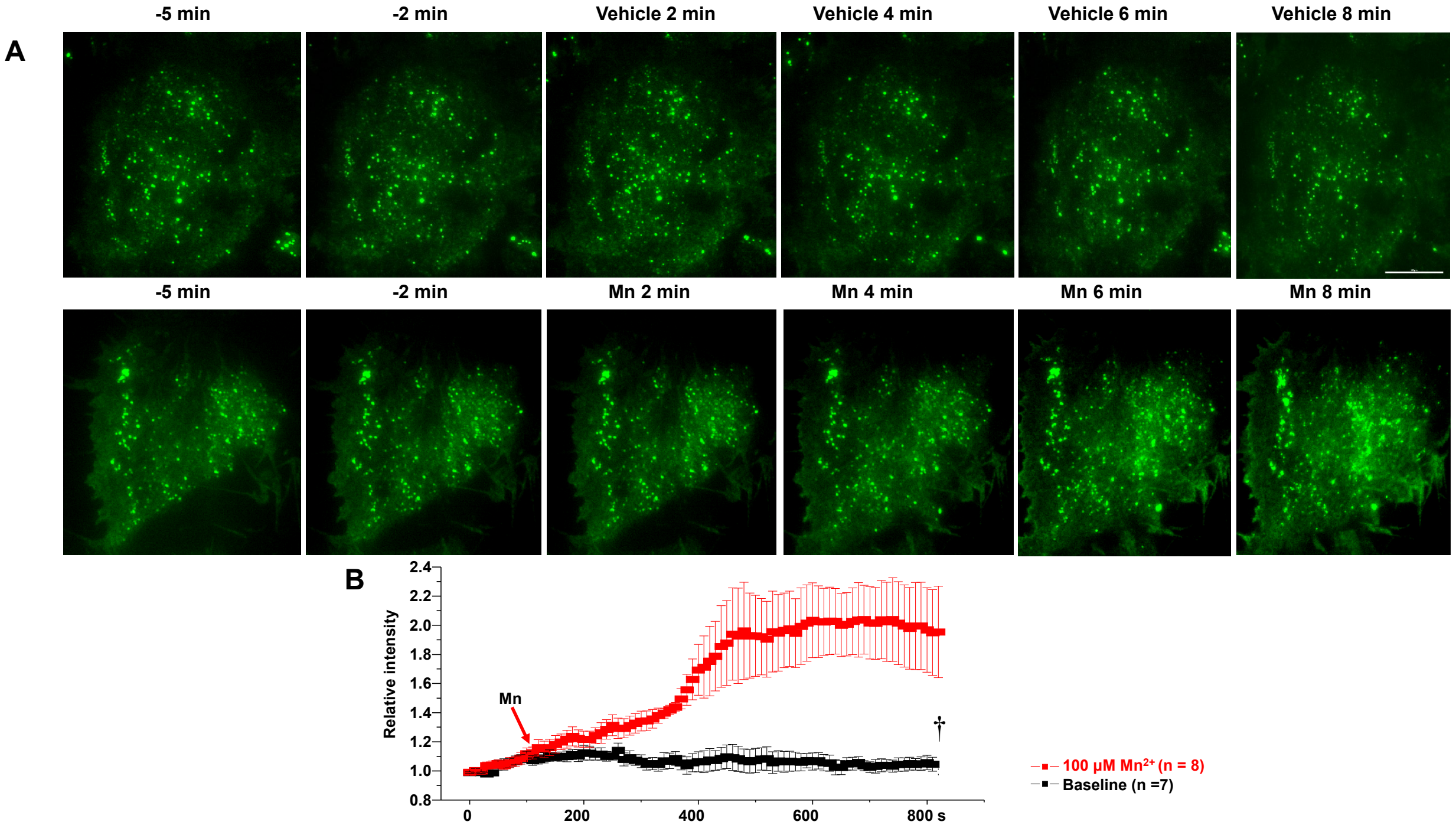
A
-5 min
-2 min
Vehicle 2 min
Vehicle 4 min
Vehicle 6 min
Vehicle 8 min
-5 min
-2 min
Mn 2 min
Mn 4 min
Mn 6 min
Mn 8 min
B
Relative intensity
2.4
2.2
2.0
1.8
1.6
1.4
1.2
1.0
0.8
Mn
0
200
400
600
800 s
100 μM Mn2+ (n = 8)
Baseline (n =7)

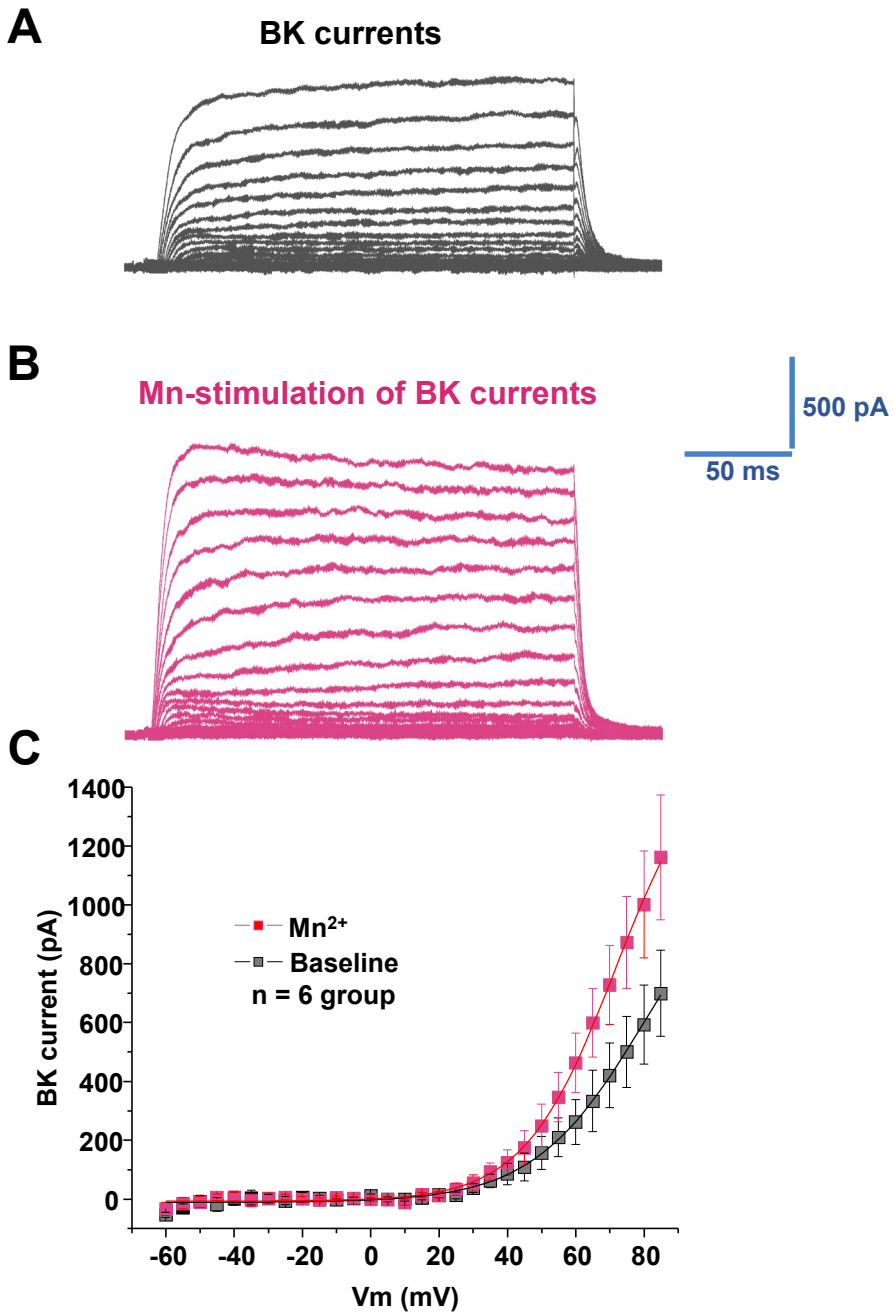
A
BK currents
B
Mn-stimulation of BK currents
500 pA
50 ms
C
1400
1200
1000
800
600
400
200
0
BK current (pA)
Mn2+
Baseline
n = 6 group
-60
-40
-20
0
20
40
60
80
Vm (mV)

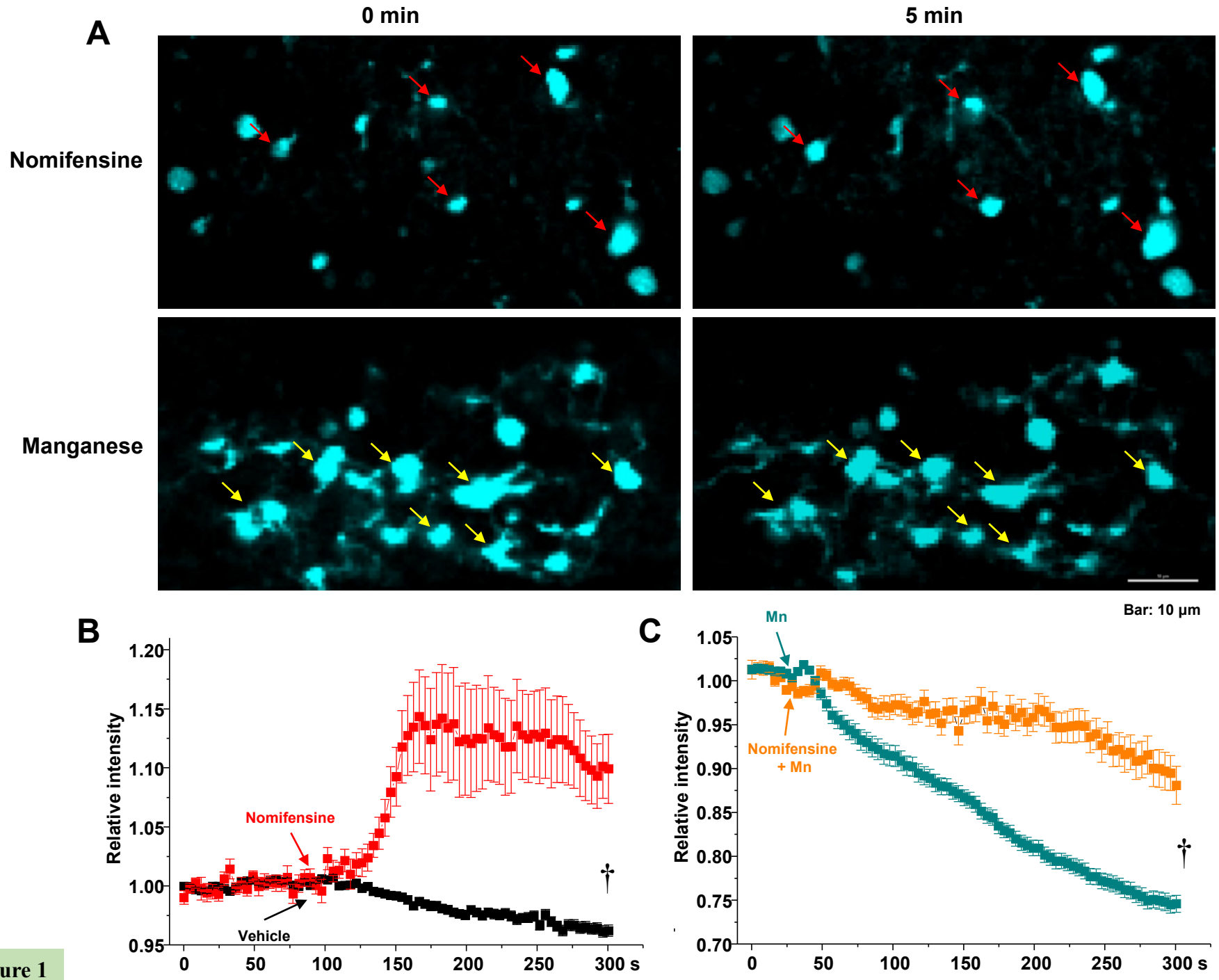


**Supplemental Figure 1**

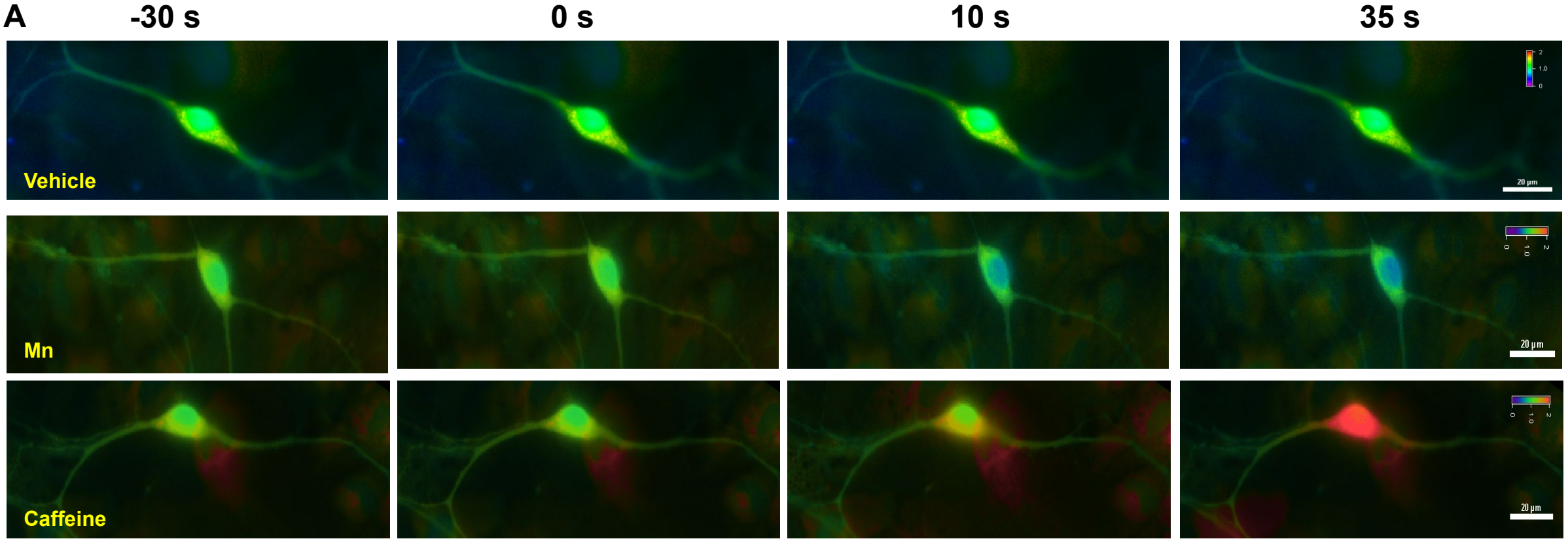


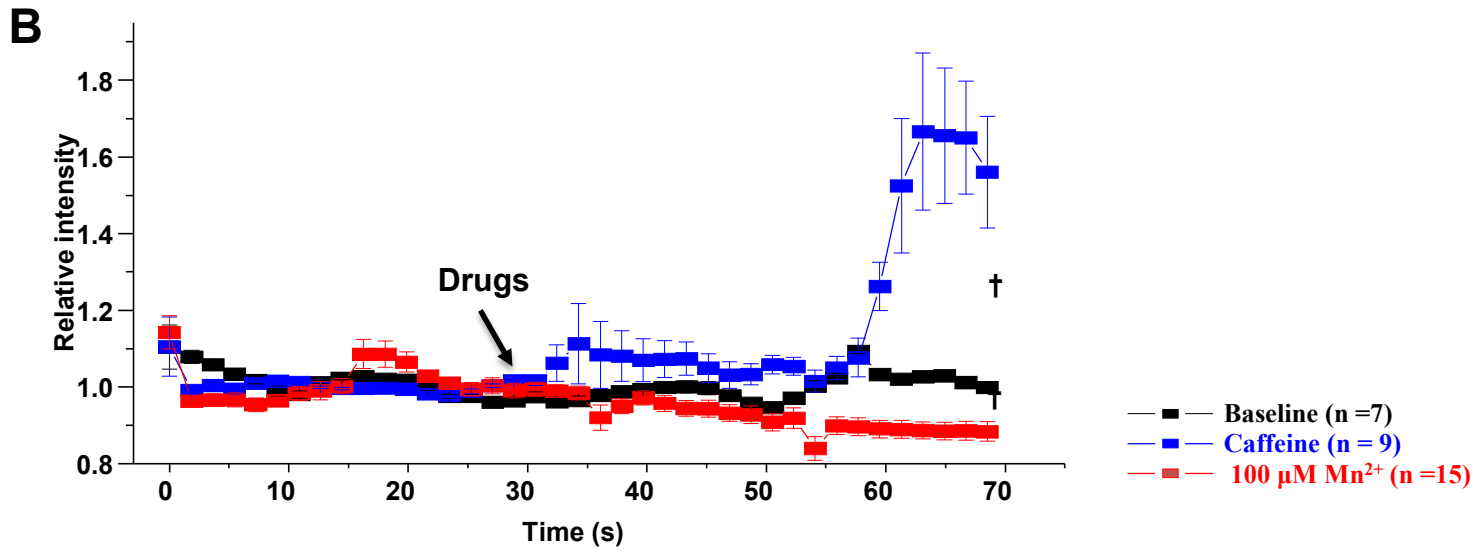


Supplemental Figure 2

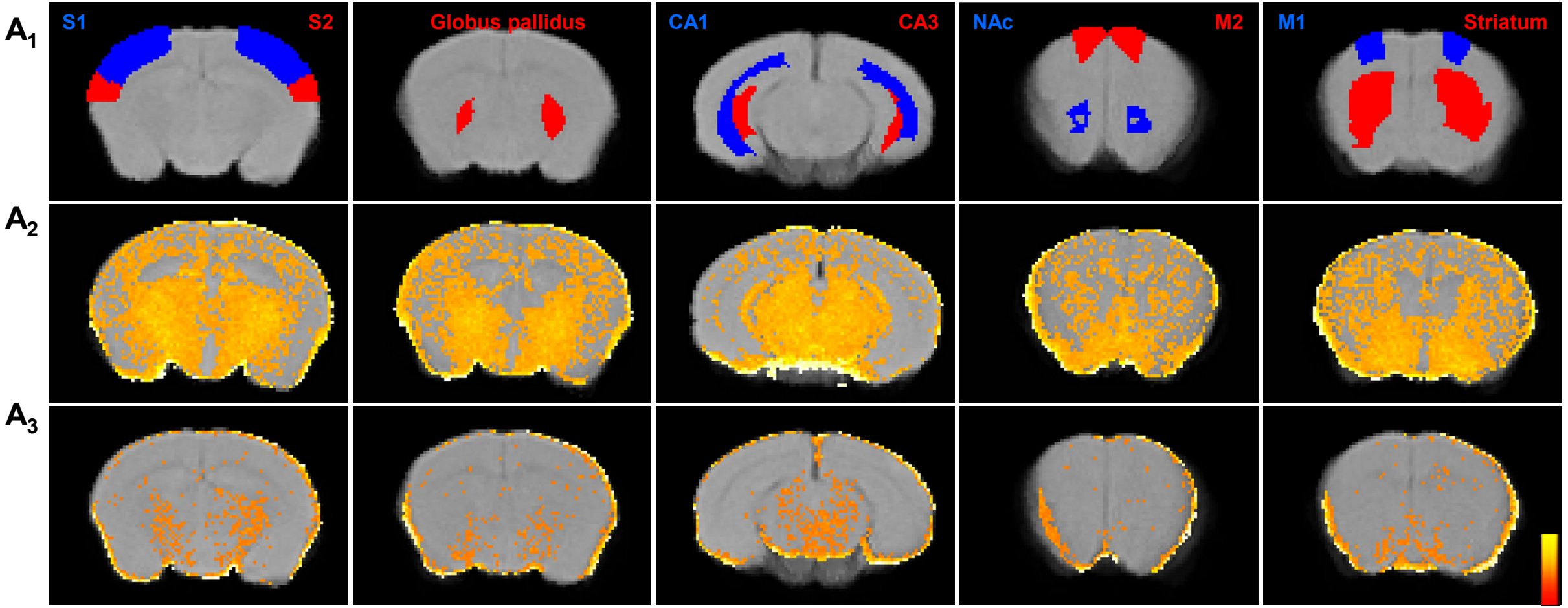


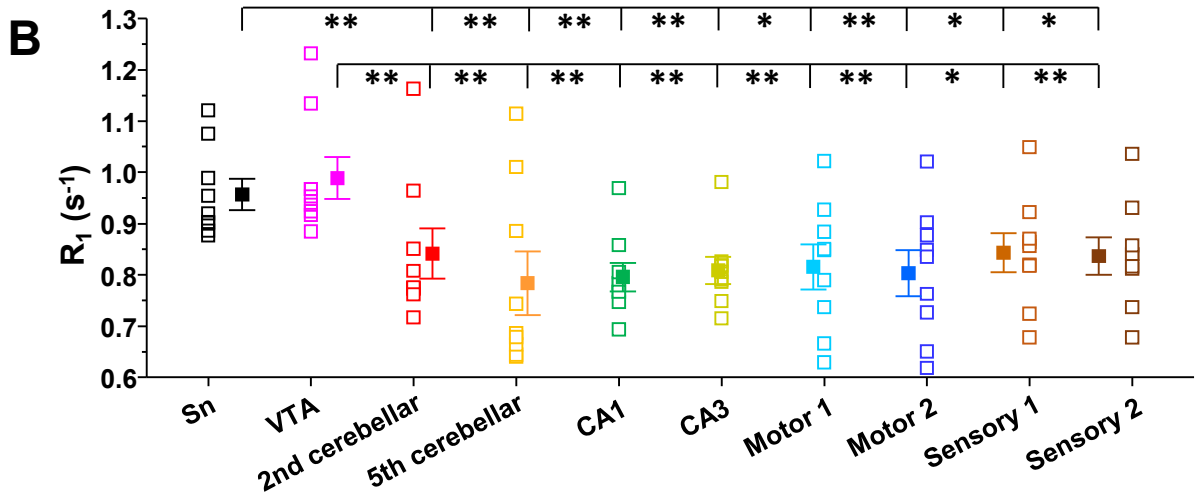


**Supplemental Figure 3**